The *in vitro* antiplasmodial and antiproliferative activity of new ferrocene-based α-aminocresols targeting hemozoin inhibition and DNA interaction

Mziyanda Mbaba,[a] Laura M.K. Dingle,[b, c] Tarryn Swart,[b, d] Devon Cash,[b, c] Dustin Laming,[b, d] Jo-Anne de la Mare,[b, c, d] Dale Taylor,[e] Heinrich C. Hoppe,[b, d] Christophe Biot,*[f] Adrienne L. Edkins,[b, c, d] Setshaba D. Khanye*[a, d, g]

[a] Faculty of Science, Department of Chemistry, Rhodes University, Grahamstown, 6140, South Africa

[b] Faculty of Science, Department of Biochemistry and Microbiology, Rhodes University, Grahamstown, 6140, South Africa

[c] Biomedical Biotechnology Research Unit, Rhodes University, Grahamstown, 6140, South Africa

[d] Centre for Chemico- and Biomedicinal Research, Rhodes University, Grahamstown, 6140, South Africa

[e] Faculty of Medicine, Division of Clinical Pharmacology, University of Cape Town, Observatory, Cape Town 7925, South Africa

[f] Univ. Lille, CNRS, UMR 8576 - UGSF - Unité de Glycobiologie Structurale et Fonctionnelle, F-59000 Lille, France

[g] Faculty of Pharmacy, Division of Pharmaceutical Chemistry, Rhodes University, Grahamstown, 6140, South Africa

Corresponding authors
Tel: +27 46 603 8397; Fax: +27 46 603 7506
E-mail addresses: s.khanye@ru.ac.za (S.D. Khanye), christophe.biot@univ-lille.fr (C. Biot)

ABSTRACT

Conjugation of organometallic complexes to known bioactive organic frameworks is a proven strategy revered for devising new drug molecules with novel modes of action. Herein, we present the *in vitro* antimalarial and antiproliferative investigation of ferrocenyl α-aminocresol conjugates assembled by amalgamation of the organometallic ferrocene unit and the α-aminocresol scaffold. The compounds pursued in the study exhibited higher toxicity towards the susceptible (3D7) and resistant (Dd2) strains of the *Plasmodium falciparum* parasite than the human HCC70 triple-negative breast cancer cell line. Indication of cross-resistance was absent for the compounds evaluated against the multi-resistant Dd2 strain. The compounds show a dual mode of action involving hemozoin inhibition and DNA interaction via minor groove binding. Lastly, compound **9a**, exhibited preferential binding for the plasmodial DNA isolated from 3D7 *P. falciparum* trophozoites over the mammalian calf thymus DNA, thereby substantiating the enhanced antimalarial activity. The presented research demonstrates the strategy of incorporating organometallic complexes into known biologically active organic scaffolds as a viable avenue to fashion novel multi-modal compounds with potential to counter drug resistance development.

INTRODUCTION

The development of resistance to clinical drugs by diseases is a grave concern that is threatening the outlook of current medicines as effective treatments in modern drug discovery and it requires innovative strategies to address. In cancer, clinical resistance develops when malignant tumour cells undergo changes at genomic and biochemical levels to counteract the effects of an administered anticancer drug. Various hypotheses explaining the processes underpinning the mechanisms that promote anticancer resistance have been proposed and are extensively presented in literature.[1-2] Succinct reviews by Housman et al. and Nikolaou et al. on cancer clinical resistance comprehensively summarize the six common mechanisms leading to development of tumoral drug resistance, of which metabolic drug deactivation and drug efflux by transmembrane proteins of cancer cells are the most prevalent.[3-4] Similarly, antimalarial drug resistance predominantly involves drug efflux and alteration of the therapeutic biomolecular target, whereby the effectiveness of the drug molecule is diminished through its accelerated removal from the active site and reduced affinity for the therapeutic target, respectively.[5-6] This is best demonstrated by the case of chloroquine resistance. The development of chloroquine resistance is postulated to be caused by altered transmembrane proteins of the parasite's digestive vacuole (DV), i.e., the active site where the drug inhibits hemozoin formation, in a manner that limits the accumulation of drug molecules in the DV due to expedited drug efflux, thus, waning its efficacy.[7-8] The challenges posed by both cancer and malarial clinical resistance present a pressing need to search for innovative bioactive molecules with potential to overcome clinical resistance.

Currently, prevailing wisdom dictates that drug candidates eliciting dual or multiple modes of action, for instance; by targeting different biological targets, may overcome or, at the very least, slow down the process of clinical resistance development.[9] To introduce mechanistic diversity into drug molecules, the hybridization approach is gaining attention in contemporary drug

discovery by merging structurally and mechanistically distinct pharmacophoric units into a single, multi-targeting molecule possessing polypharmacophoric moieties.[10-11] Particularly, the incorporation of organometallic units into bioactive organic drug scaffolds is touted as a promising strategy to produce novel bioactive agents with multiple modes of action.[12-13] Mechanistically, this is due to the fact that organometallic units such as ferrocene possess desirable medicinal attributes, including high lipophilicity and reversible redox character as well as peculiar modalities, that become engendered into the resulting hybrid molecule, leading to the attainment of multitargeting agents.[12-14] Moreover, the next generation antimalarial drug ferroquine, a chloroquinoline-ferrocene conjugate, is a promising candidate for cancer repositioning possessing better efficacy against prostate cancer cell lines than its parental compound, chloroquine, by targeting autophagy and lysosomal function.[15] Recently, the research teams of Cohen and Metzler-Nolte reported the first library of small, three-dimensional (3D) metallofragments, which included ferrocene, that showed significant inhibitory activity against a selection of therapeutic targets that are relevant in cancer (Hsp90), viral (PA_N) malignancies and bacterial (NDM-1) infections.[16] This seminal work accentuates the medicinal potential of metal-based compounds. Furthermore, the intrinsic 3D shape of organometallic units is hypothesized to facilitate the binding capacity of these molecular fragments to 3D spaces in biological receptors better than the conventional predominantly 2D organic molecules due to improved structural affinity.[16-17]

The α-aminocresols belong to a class of small phenolic compounds with proven biological activity going as far back as 1946 (**Figure 1**).[18] Burkhalter and co-workers were among the first to investigate the antimalarial efficacy of α-amino-*o*-cresols of the type represented by the parental structure **1**, resulting in the identification of hit compound **2** with substantial *in vivo* antimalarial activity in avian models.[18] Subsequently, Schmidt and Crosby demonstrated that biphenyl α-amino-*o*-cresol (**3**) reduced the burden of malaria in infected monkeys.[19]

Additionally, α-aminocresols have attracted renewed research interest in the recent years as antimalarial agents.[20-21] By conjugating the adamantane motif to the α-aminocresol scaffold, Chinnapattu et al. generated a series of adamantane aminomethylphenols (**4**) with 3D geometry possessing impressive plasmocidal activity against chemosusceptible (NF54) and multidrug-resistant (K1) *Plasmodium falciparum* strains in the nanomolar range.[20] Similarly, Chibale and co-workers incorporated the α-aminocresol moiety into the benzimidazole scaffold to produce α-aminocresol-benzimidazole conjugates (**5**) that were active against the same strains of the malaria parasite.[21] Several α-aminocresol derivatives are featured in the Open-Access Box of Medicines for Malaria Venture (MMV) as important structural motifs for investigation and development in antimalarial drug research.[22] Despite these successes, there are no accounts of organometallic derivatives of the α-amino-*o*-cresol scaffold presented in literature to our knowledge.

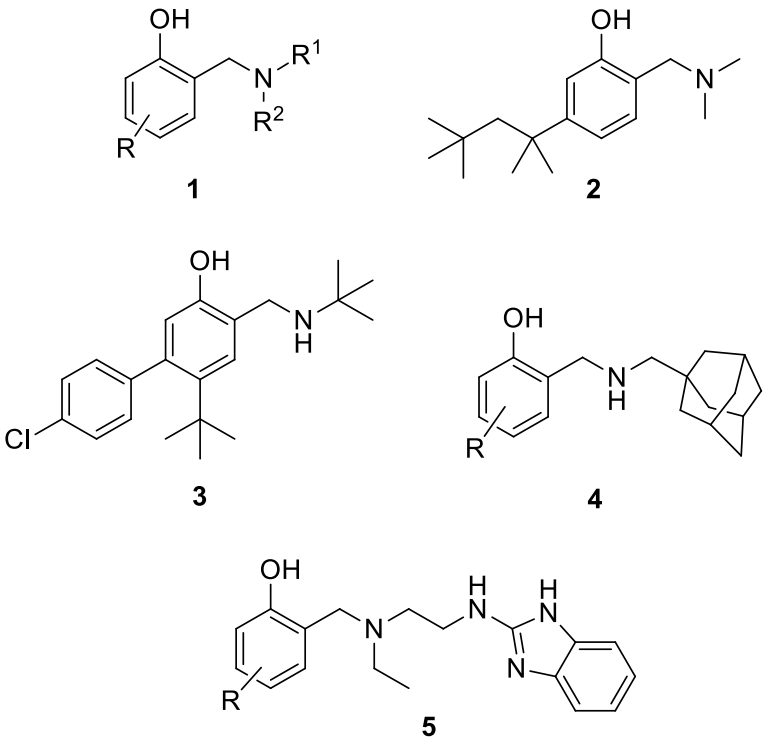

Figure 1 Chemical structures of α-aminocresol with antimalarial activity.

Previously, we reported the medicinal potential of ferrocenyl 1,3-benzoxazines as multi-active agents possessing *in vitro* antiproliferative, antiplasmodial and antitrypanosomal efficacy.[23] Our attempts to synthesize ferrocenyl 1,3-benzoxazine **8** by Mannich condensation of 6-bromophenol (**6**) with ferrocenyl amine **7a** and paraformaldehyde led to concomitant formation of the α-aminocresol side product **9a**, which displayed comparable anticancer and antimalarial potencies to the targeted benzoxazine product (**8**) when screened for biological activity (**Scheme 1**).

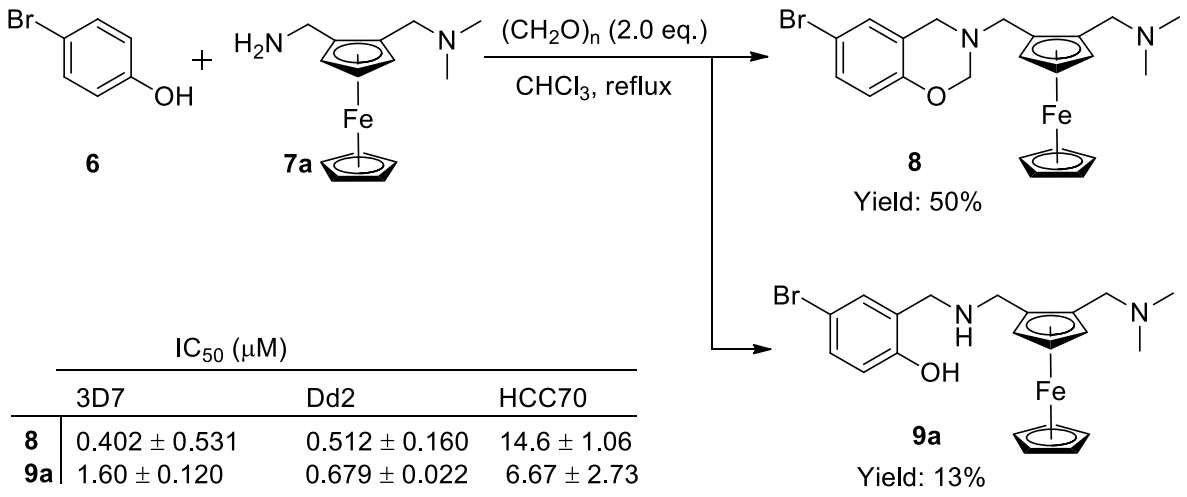

	IC$_{50}$ (μM)		
	3D7	Dd2	HCC70
8	0.402 ± 0.531	0.512 ± 0.160	14.6 ± 1.06
9a	1.60 ± 0.120	0.679 ± 0.022	6.67 ± 2.73

Scheme 1 Synthesis of ferrocenyl 1,3-benzoxazine **8** leading to concomitant formation of ferrocenyl α-aminocresol **9a** presented with the corresponding biological efficacies (IC_{50} values) of the compounds.

Inspired by these observations and the biological potential of the α-aminocresol scaffold reported in literature together with the pharmacological benefits of incorporating the organometallic ferrocene unit into bioactive organic compounds, the current study explores the *in vitro* anticancer and antimalarial activity of ferrocenyl α-amino-*o*-cresol derivatives. Furthermore, investigation of the pursued compounds for hemozoin inhibitory activity, which is a therapeutic target of choice for several antimalarial compounds, and DNA binding affinity,

both experimentally and by *in silico* docking simulations, suggested that the compounds likely exhibit biological activity by targeting hemozoin formation and DNA alkylation.

RESULTS AND DISCUSSION

Synthesis

In order to determine the pharmacological profile of ferrocenyl α-aminocresols, ferrocenyl amine **7a** and its less basic congener **7b** lacking the protonatable CH_2NMe_2 side chain were synthesized according to methods reported in literature.[24] The basic ferrocenyl CH_2NMe_2 moiety is known to enhance the antiplasmodial activity of ferrocene-based compounds.[23-25] Thus, it was considered prudent to synthesize both α-aminocresol analogues endowed with and devoid of this functionality to provide insights into the pharmacological effects of modifying the ferrocene unit on the biological activity of the resultant compounds. To avoid possible formation of the benzoxazine product, the target ferrocenyl α-aminocresol derivatives were assembled by reductive amination of substituted benzaldehydes (**10a-h**) with ferrocenyl amines **7a-b** using sodium borohydride as the reductant to exclusively yield the desired products.[26] Briefly, a suspension of a substituted benzaldehyde **10a-h** and amine **7a-b** in ethanol was refluxed for 4 – 5 hours to produce an imine intermediate *in situ* that was subsequently subjected to reduction with sodium borohydride to furnish the desired compounds **9a-m** in moderate to excellent yields following a simple acid-base workup (**Scheme 2**).[26] The amine **7b** lacking the CH_2NMe_2 side chain on the ferrocene unit effected higher product yields than amine **7a** endowed with this moiety, meanwhile the nature of the benzene substituents (R^1) did not seem to have an obvious influence on the product yields. For instance, despite having the same benzene substituents (R^1 = 4-Br, 6-NO_2), compound **9m** prepared from amine **7b** was achieved at 82% yield compared to its ferrocenyl CH_2NMe_2 congener **9h** synthesized from amine **7a** with a yield of 23%.

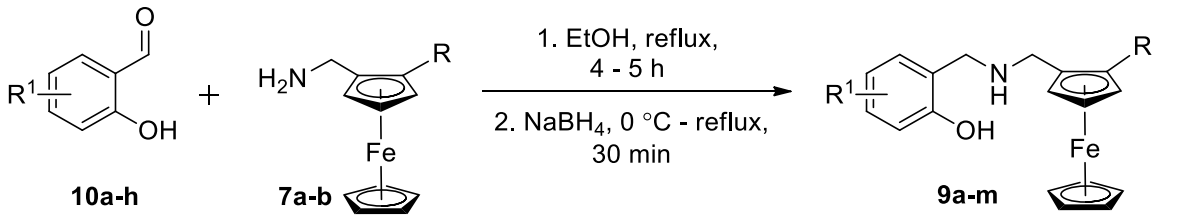

10a-h **7a-b** **9a-m**

10a : R^1 = Br
10b : R^1 = 4-Me
10c : R^1 = 4-NO_2
10d : R^1 = H
10e : R^1 = 6-OMe
10f : R^1 = 6-NO_2
10g : R^1 = 4,6-Br
10h : R^1 = 4-Br, 6-NO_2

7a: R = CH_2NMe_2
7b: R = H

	R^1	Isolated yield (%)
R = CH_2NMe_2	**9a** : 4-Br	41
	9b : 4-Me	38
	9c : 4-NO_2	35
	9d : H	63
	9e : 6-OMe	76
	9f : 6-NO_2	38
	9g : 4,6-Br	43
	9h : 4-Br, 6-NO_2	23
R = H	**9i** : H	98
	9j : 4-Br	97
	9k : 6-NO_2	96
	9l : 4,6-Br	71
	9m : 4-Br, 6-NO_2	82

Scheme 2 Synthesis of target ferrocenyl α-aminocresols by reductive amination.

The biological activity of α-aminocresols is attributed to the molecular architecture of the scaffold. Particularly, the exhibition of the internal hydrogen bond between the phenolic hydroxyl and amino nitrogen groups is crucial for the antiplasmodial activity of α-aminocresols.[21] Additionally, Chinnapattu et al. found that constraining the rotatability of the bond between the α-carbon and the amino nitrogen atom by introducing an amide bond led to a decrease in activity of the resulting compounds.[20] Therefore, in order to comprehensively elucidate the structure-activity relationship (SAR) profile of the pursued ferrocenyl α-aminocresols, the phenolic hydroxy group (OH) and the rotatable α-C–NH bond were modified by synthesizing non-phenolic benzylamines **12a-d** and salicylamides **14a-g** as non-rotatable aminocresol congeners, respectively.

The non-phenolic benzylamines **12a-c** were prepared by replacing the phenolic OH group with substituents; H, OMe, and NO_2, from appropriate benzaldehydes **11a-c** and ferrocenyl amine

7a following the synthetic route in **Scheme 3**. The 2-aminobenzylamine **12d** was obtained via zinc-catalyzed reduction of 2-nitrobenzylamine **12c** in the presence of ammonium chloride.[27] We envisaged that substituting the phenolic OH group of the α-amino-*o*-cresol scaffold for these functional groups would disrupt the intramolecular hydrogen bonding in the resulting compounds and provide understanding of the pharmacological significance of this molecular feature.

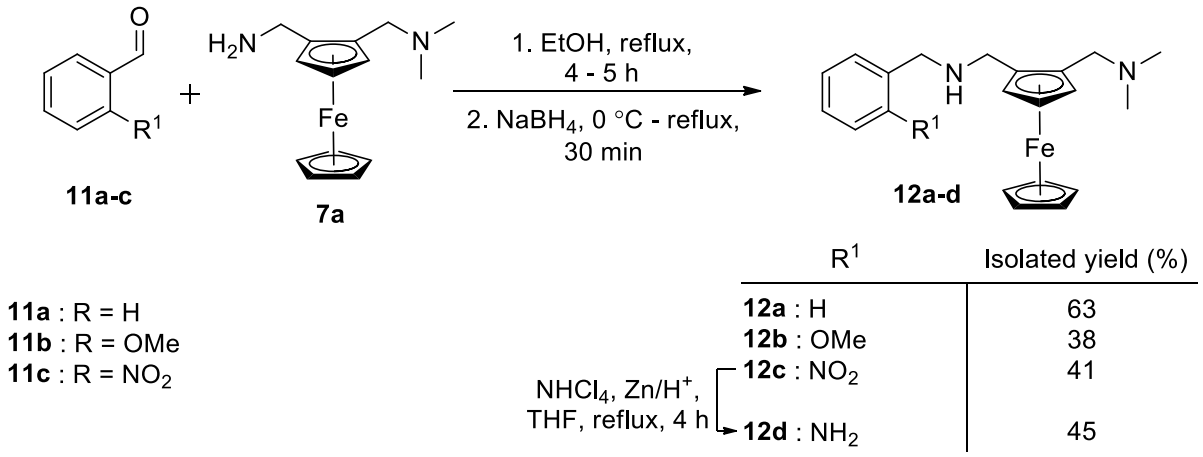

R^1	Isolated yield (%)
12a : H	63
12b : OMe	38
12c : NO_2	41
12d : NH_2	45

Scheme 3 Synthesis of non-phenolic ferrocenyl benzylamines **12a-d**.

Similarly, salicylic acids **13a-e** and ferrocenyl amines **7a-b** were coupled by *N,N'*-dicyclohexylcarbodiimide (DCC) amidation in one step under microwave irradiation in pyridine (**Scheme 4**).[28] To further probe the biological effect of modifying the benzene ring, ferrocenyl nicotinamide **14f** containing a pyridine ring in lieu of the benzene ring was synthesized from nicotinic acid **13e** and ferrocenyl amine **7a**. Moreover, it was considered worthwhile to investigate the influence of the phenolic OH group within this series by exchanging it with a more acidic thiol functionality (SH). Thus, a thiol congener of salicylamide **14f** was synthesized by reacting thiosalicylic acid **13f** and ferrocenyl amine **7b** to produce thiosalicylamide **14g** featuring the SH group in position 2 (**Scheme 4**).

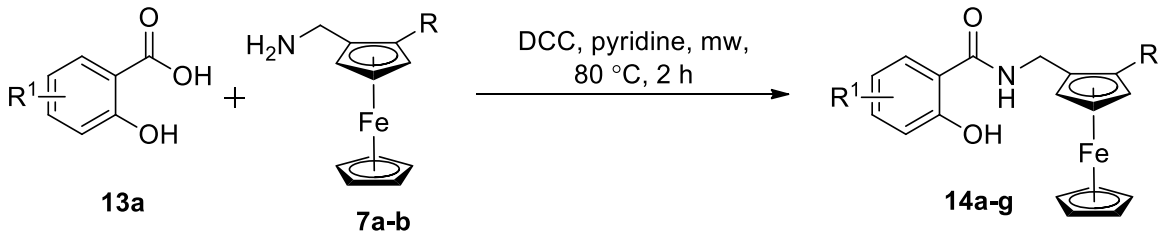

13a : R^1 = H
13b : R^1 = 5-Cl
13c : R^1 = 5-NO_2
13d : R^1 = 4-F
13e : R^1 = H*
13f : R^1 = H**

7a: R = CH_2NMe_2
7b: R = H

	R^1	Isolated yield (%)
R = CH_2NMe_2	**14a** : H	92
	14b : 5-Cl	95
	14c : 5-NO_2	78
	14d : 4-F	82
	14e : H*	69
R = H	**14f** : H	70
	14g : H**	68

Scheme 4 Synthesis of ferrocenyl salicylamide **14a-g**. **13e**: R^1 = H*, 2-hydroxynicotinic acid. **13f**: R^1 = H**, thiosalicylic acid. **14e**: R^1 = H*, 2-hydroxynicotinamide product synthesized from **13e**. **14g**: R^1 = H**, thiosalicylamide product synthesized from **13f**.

The structural identities of all the synthesized compounds were confirmed by common spectroscopic techniques: nuclear magnetic resonance (^{1}H and ^{13}C NMR) and high-resolution mass spectrometry (HRMS). The full spectral data of all the compounds are provided in the experimental section and **Supporting Information** of this paper. For all the compounds, the most notable characteristics of their ^{1}H NMR spectra was the appearance of the phenolic protons in the aromatic region and the distinctive ferrocene signals at δ 4.50 – 4.00 ppm. The ferrocene signals were observed as three broad singlets for the CH_2NMe_2 ferrocenyl compounds (**9a-h**, **12a-d** and **14a-e**) each integrating for one proton or as two 2H triplets in the case of plain ferrocenyl congeners (**9i-m** and **14f-g**) and a 5H singlet corresponding to the top and bottom cyclopentadienyl rings, respectively. Also noteworthy was the splitting of the two ferrocene-appended methylene (CH_2) protons that were both observed as two 1H doublets due to geminal coupling (*J*-coupling constants: 12.0 – 13.6 Hz) and planar chirality of the ferrocene unit for the CH_2NMe_2-containing derivatives (**9a-h**, **12a-d** and **14a-e**).[24] The purity of the compounds was determined by HPLC (see **Supporting Information**) and the values were

uncorrected. The HPLC purity, which was at least 80% in all instances, together with the clean ^{1}H and ^{13}C NMR spectra of the compounds were convincing to suggest adequate purity to proceed with biological evaluation assays.

Biological evaluation

The synthesized ferrocenyl α-aminocresols were evaluated for potential antiplasmodial and anticancer activity *in vitro* against the chloroquine-sensitive (CQS) 3D7 *P. falciparum* strain and human HCC70 triple-negative breast cancer cell line. A selection of the compounds was also assessed on the chloroquine-resistant (CQR) Dd2 *P. falciparum* strain. Furthermore, to establish the possible mode of action of the ferrocenyl α-aminocresols, representative compounds from each series showing the most promising activity were studied for DNA binding affinity and hemozoin inhibition in terms of the β-hematin binding assay employing spectrophotometric techniques from literature.[29-30] The findings of the mechanistic studies were corroborated by *in silico* docking simulations of the tested compounds against a B-DNA structure and a homology model of the hemozoin crystal using AutoDock Vina (v1.5.6, 2014).[31]

In vitro antiplasmodial activity

The antiplasmodial activity of the compounds was determined on the chloroquine-sensitive (CQS) 3D7 and chloroquine-resistant (CQR) Dd2 *P. falciparum* strains by at least two independent replicates. In each experiment, varying concentrations of the test compound were incubated with the parasites for 48 hours and the activity was determined as the mean of effective concentration required to reduce *P. falciparum* parasitemia (assessed by Plasmodium lactate dehydrogenase activity) 50%, i.e., half-maximal concentration (IC_{50} value). Known antimalarial drugs, chloroquine (CQ) and artemisinin (Art) were assessed similarly to the test compounds and used as positive controls in the biological evaluation assays. The results of the antiplasmodial screening assay are presented in **Table 1**. The IC_{50} values are reported as a mean value obtained from triplicate experiments for each compound with the margin of error estimated by the standard deviation (± SD).

Table 1 *In vitro* antiplasmodial activity of ferrocenyl α-aminocresol derivatives evaluated against the CQS 3D7 and CQR Dd2 *P. falciparum* strains.

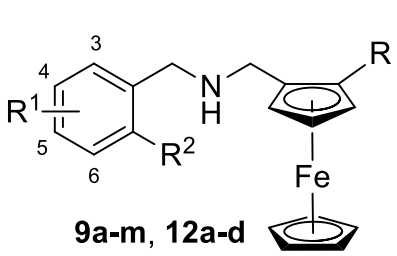

9a-m, **12a-d**

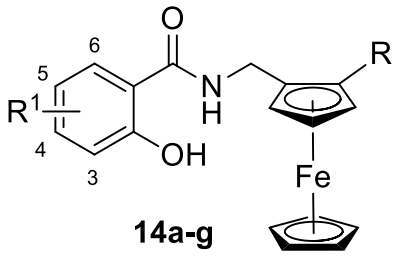

14a-g

Compound	R	R^1	R^2	IC_{50} (μM)		R.I.[a]
				3D7	Dd2	
9a	CH_2NMe_2	4-Br	OH	1.60 ± 0.04	**0.69 ± 0.02**	0.4
9b	CH_2NMe_2	4-Me	OH	**0.98 ± 0.10**	nd	–
9c	CH_2NMe_2	4-NO_2	OH	1.88 ± 0.10	nd	–
9d	CH_2NMe_2	H	OH	2.23 ± 0.12	nd	–
9e	CH_2NMe_2	6-OMe	OH	4.70 ± 0.25	6.61 ± 1.74	1.4
9f	CH_2NMe_2	6-NO_2	OH	12.3 ± 0.24	nd	–
9g	CH_2NMe_2	4,6-Br	OH	1.10 ± 0.14	**0.94 ± 0.08**	0.9
9h	CH_2NMe_2	4-Br, 6-NO_2	OH	5.52 ± 0.30	nd	–
9i	H	H	OH	nd	nd	–
9j	H	4-Br	OH	2.30 ± 0.28	1.68 ± 0.28	0.7
9k	H	6-NO_2	OH	nd	nd	–
9l	H	4,6-Br	OH	4.30 ± 0.03	3.87 ± 0.21	0.9
9m	H	4-Br, 6-NO_2	OH	nd	>10	–
12a	CH_2NMe_2	H	H	2.99 ± 0.30	nd	–
12b	CH_2NMe_2	H	OMe	4.78 ± 0.23	nd	–
12c	CH_2NMe_2	H	NO_2	3.13 ± 0.39	nd	–
12d	CH_2NMe_2	H	NH_2	4.49 ± 0.39	nd	–
14a	CH_2NMe_2	H	OH	9.64 ± 1.17	nd	–
14b	CH_2NMe_2	5-Cl	OH	20.9 ± 0.85	nd	–
14c	CH_2NMe_2	5-NO_2	OH	12.8 ± 0.85	nd	–
14d	CH_2NMe_2	4-F	OH	na	nd	–
14e[b]	CH_2NMe_2	H	OH	21.9 ± 1.47	nd	–
14f	H	H	OH	na	nd	–
14g[c]	H	H	SH	na	nd	–
CQ	–	–	–	0.03 ± 0.0	0.188 ± 0.07	6.3
Art	–	–	–	–	0.006 ± 0.0	–

R.I.[a] = resistance index, ratio of activity against the resistant strain to activity against the sensitive strain, i.e., IC_{50}[Dd2]/IC_{50}[3D7]. **14e**[b] = nicotinamide congener. **14g**[c] = thiosalicylamide analogue. nd = not determined. na = not active.

From the antiplasmodial evaluation results, the α-amino-*o*-cresol series **9a-m** was generally the most potent against the 3D7 *P. falciparum* strain among the screened compounds followed by benzylamines **12a-d** and salicylamides **14a-g**, respectively. In all cases the basic CH_2NMe_2 ferrocenyl derivatives were more potent than their less basic analogues devoid of this motif. This observation corroborates the favourable pharmacological effects of attaching the CH_2NMe_2 moiety to the ferrocene unit as observed in previous studies.[23-24]

For the α-amino-*o*-cresol series **9a-m**, the electron-donating groups (EDGs) on the benzene ring appeared to impart higher efficacy with Me > Br > NO_2 irrespective of the position of substitution on the benzene ring (**Table 1**). For instance, compounds bearing the electron-releasing methyl and methoxy groups (**9b** and **9e**) exhibited higher activity than their nitro-containing counterparts (**9c** and **9f**) by approximately 2-fold. Aminocresol **9b** containing the electron-donating methyl group emerged as the most potent compound against the CQS 3D7 strain in the entire series with an IC_{50} value of 0.98 ± 0.10 μM followed by compound containing electron-withdrawing groups (EWGs): Br (**9a**) and NO_2 (**9d**), respectively. Substitution at C-4 (**9a-d**) was more favourable for antiplasmodial activity compared to position 6 (**9e-f**), while simultaneous functionalisation of these positions (**9g-h**) was only tolerated for efficacy. As before, of the six compounds from the aminocresol series tested against the Dd2 multi-resistant strain, the brominated compounds (**9a** and **9g**) with the basic CH_2NMe_2 moiety appended on the ferrocenyl unit were the most active with comparable IC_{50} values in the sub-micromolar range, whereas their less basic congeners devoid of this moiety (**9j** and **9l**) displayed activity in the low micro-molar range (**Table 1**). As with the susceptible 3D7 strain, substitution at C-6 (*ortho*-position) proved detrimental for the antiplasmodial activity against the resistant Dd2 strain compared to C-4 (*para*-position). This is illustrated by the inferior activity of the 6-OMe aminocresol **9f** (IC_{50} = 6.61 ± 1.74 μM) with respect to the derivatives containing at least one Br group on C-4 (**9a**, **9g**, **9j** and **9l**) (**Table 1**).

The antiplasmodial activity of the α-aminocresol **9d** was reduced upon removal (**12a**) and replacement of the phenolic OH group with the OMe (**12b**), NO_2 (**12c**) and NH_2 (**12d**) functionalities by almost 2-fold (**Table 1**), highlighting the pharmacological significance of this structural feature. The reduction in activity due to the replacement of the OH group, could be explained by the influence of the internal hydrogen bond (O–H···N–H) on the antimalarial activity of α-aminocresols. Indeed, the presence of the intramolecular hydrogen bond is known to augment the activity of antimalarial agents.[21, 32-34] The intramolecular hydrogen bond in the α-aminocresol side chain of 4-aminoquinoline antimalarial drugs, amodiaquine and isodiaquine, is believed to be crucial for their activity.[32] Moreover, Madrid et al. demonstrated that incorporating the intramolecular hydrogen bond of α-aminocresol into the side chain of 4-aminoquinolines enhances their activity against the drug-resistant *P. falciparum* strains.[33] Thus, the observed reduction in antiplasmodial activity of the ferrocenyl non-cresol benzylamine derivatives **12a-d** seems to be a result of removing (**12a**) and replacing the acidic, strong hydrogen bond donor, i.e., phenolic OH group (**9d**), with hydrogen bond acceptors OMe (**12b**) and NO_2 (**12c**) and basic donor NH_2 (**12d**), leading to reduced activity due to formation of a weaker hydrogen bond between these groups and the aliphatic NH group.

Constraining the rotation of the C–N bond between the α-carbon and NH group was unfavourable for antiplasmodial activity as demonstrated by the substantially inferior potency of ferrocenyl salicylamides **14a-g** relative to α-aminocresols **9a-m** and non-cresol benzylamines **12a-d** (**Table 2**). This is further supported by the findings of Chinnapattu et al. in which they found that incorporating the amide bond between the α-carbon and NH group in adamantane-based aminocresols caused their antimalarial potency to plummet.[20] Within the salicylamide series, the unsubstituted analogue **14a** was the most active, while the 5-Cl (**14b**) and 5-NO_2 (**14c**) variants substituted *para* with respect to the OH group were less active. Activity was lost upon substitution of the fluorine atom in the *meta*-position relative to OH,

emphasizing the pharmacological significance of *para*-substitution as previously observed for the aminocresols **9a-m** (**Table 1**). The nicotinamide congener **14e** was half as potent as the parental salicylamide **14a**. This suggests that replacing the benzene ring with the pyridine unit is undesirable for antiplasmodial activity. Lastly, salicylamide **14f** and thiosalicyalmide **14g** lacking the basic CH_2NMe_2 ferrocenyl chain were ineffective at inhibiting the growth of the 3D7 strain at the tested concentrations.

To investigate the selectivity of the compounds between the *P. falciparum* parasite and human cells, HeLa cells were employed to assess the general toxicity of the compounds using a resazurin assay as described in previous studies in literature.[35-36] The compounds were tested at a fixed concentration of 20 μM and the results are illustrated in **Figure S1** plotted in parallel with the viability of 3D7 *P. falciparum* parasitaemia. At least 70% HeLa cell viability was observed for the majority of compounds at the tested concentration of 20 μM, implying preferential selectivity for the malaria parasite over mammalian cells.

Antiproliferative activity

The *in vitro* anticancer efficacy of a selection of the investigated compounds was determined on the HCC70 triple-negative breast cancer cell line. In a typical procedure, live cells were treated with varying concentrations of test compounds or anticancer drug paclitaxel and then incubated for a period of 48 – 72 hours. Antiproliferative activities were determined using the resazurin assay in triplicate and reported as half-maximal inhibitory concentrations, i.e., IC_{50} values (**Table 2**).

Table 2 *In vitro* antiproliferative activity of ferrocenyl α-aminocresol derivatives evaluated against the HCC70 human triple-negative breast cancer cell line.

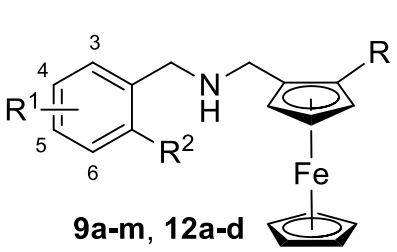

9a-m, **12a-d**

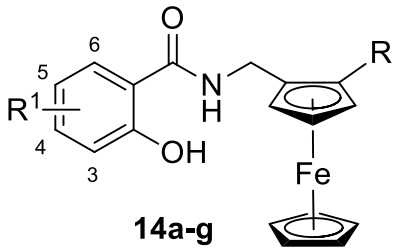

14a-g

Compound	**R**	**R^1**	**R^2**	**IC_{50} (μM)**[a]
				HCC70
9a	CH_2NMe_2	4-Br	OH	6.67
9b	CH_2NMe_2	4-Me	OH	28.4
9h	CH_2NMe_2	4-Br, 6-NO_2	OH	56.2
9l	H	4,6-Br	OH	24.2
12b	CH_2NMe_2	H	OMe	20.9
Paclitaxel	–	–	–	0.0025

IC_{50} (μM)[a] = half-maximal inhibitory concentration determined in triplicate, in all cases the standard deviation (±SD) was below 2.0.

For all tested compounds, only three α-amino-*o*-cresols (**9a**, **9b** and **9h**) carrying the ferrocenyl CH_2NMe_2 and the *O*-methyl α-amino-*o*-cresol **12b** were active against the HCC70 cell line with IC_{50} values between 6.67 and 56.2 μM (**Table 2**), highlighting the importance of the CH_2Me_2 motif as before. Compound **9l** lacking the basic ferrocenyl CH_2NMe_2 motif was an exception to this observation and exhibited antiproliferative activity with an IC_{50} value of 24.2 μM. All the compounds not presented in **Table 2** were non-toxic towards the cell line. Notably, the activity was lost upon removal of the *ortho* oxygen atom in the α-amino-*o*-cresol template (**12a**). Likewise, rigidifying the C–NH bond in salicylamides (**14a-f**) was detrimental for anticancer activity of the compounds as no activity was observed for these compounds. This corroborates the patterns noted in the biological activity of plasmocidal adamantane-based α-amino-*o*-cresols by Chinnapattu et al.[20]

Mechanistic studies

Based on the *in vitro* biological screening results, the investigated compounds exhibited higher selectivity for both the 3D7 and Dd2 *P. falciparum* parasites over the mammalian HCC70 triple-negative breast cancer cell line. As with the majority of antiplasmodial compounds, particularly 4-aminoquinines, that exert biological activity by targeting the heme detoxification pathway, i.e., hemozoin formation, we envisaged that our α-amino-*o*-cresol derivatives might possess a similar ability.[37] Moreover, we previously demonstrated that related Mannich bases, i.e., ferrocenyl 1,3-benzoxazines, exhibited biological activity involving DNA interaction leading to DNA damage.[23] As Mannich base derivatives, we postulated that the investigated α-amino-*o*-cresol analogues in the current study would display activity similar to the 1,3-benzoxazines through DNA interaction.[23] Thus, representative compounds from each series showing the most encouraging activity were probed for DNA binding affinity determined by UV-Vis spectroscopic procedures and hemozoin inhibition using the β-hematin binding assay from literature.[29-30] The obtained results were validated by performing *in silico* docking simulations of the compounds against a constructed hemozoin crystal model and a B-DNA structure from protein data bank.

β-Hematin binding assay for hemozoin inhibition

The inhibition of the hemozoin crystallization pathway is a commonplace mechanism by which most compounds exhibit antimalarial activity. The assay developed by Ncokazi and Egan making use of β-hematin, a synthetic form of hemozoin, is an invaluable tool in the screening of antimalarial agents for hemozoin inhibition.[30] In the β-hematin binding assay, a homogeneous suspension of β-hematin was treated with varying concentrations of representative compounds: α-amino-*o*-cresols **9a**, **9b** and **9j**, amine **12a** and salicylamide **14a**, and CQ as a positive control in a 96-well plate. Crystallization of β-hematin into hemozoin was

induced by addition of NP-40 detergent into each well followed by a 6-hour incubation at 37 °C. The hemozoin inhibition capacity of the compounds was determined by assessing the absorbance of the free heme complex at 405 nm for each concentration according to the pyridine-ferrichrome method.[38] The results were reported as IC_{50} values generated by non-linear regression analysis of a plot of absorbance vs. log [compound concentration] in GraphPad Prism 4.0 (**Table 3**).

Table 3 Results of the β-hematin binding assay for hemozoin inhibition and calculated partition coefficients (*C*logP).

Compound	**IC_{50} (μM)**[a]	***C*logP**[b]
9a	88.7 ± 1.04	4.67
9b	230.1 ± 1.08	4.24
9j	81.7 ± 1.03	4.97
12a	> 500	3.81
14a	194.4 ± 1.05	3.52
CQ	328.8 ± 1.08	–

IC_{50}[a] = concentration of compound required to inhibit crystallization of hematin to hemozoin by half of its initial concentration, the margin of error is reported as the standard error. *C*logP[b] = calculated partition coefficients, values were calculated according the procedure reported in ref. [39] for logP prediction of ferrocenyl compounds (**Supporting Information**). The prediction does not take into account intramolecular hydrogen bonding effects.

The brominated α-amino-*o*-cresols **9a** and **9j** showed the highest binding affinity for β-hematin as demonstrated by their comparable IC_{50} values of 88.7 and 81.7 μM, respectively. Compound **9b** bearing the methyl group in place of the bromine had a lower affinity relative to the brominated aminocresols, implying that the bromine atom at C-4 may be conducive for binding to the heme complex. Inhibition of hemozoin was lost upon removal of the phenolic OH group in compound **12a** as suggested by its inferior activity (IC_{50} > 500 μM). Based on this observation, it was apparent that the intramolecular hydrogen bond in aminocresols is not only

crucial for the antiplasmodial activity of the compounds but is also associated with their ability to interact with the *P. falciparum* target, hemozoin. The effects of the amide bond were unfavourable for hemozoin inhibitory activity of salicylamide **14a** as similarly observed for the antiplasmodial activity. Moreover, it was interesting to note that the observed hemozoin inhibitory activity seemed to be correlated to the lipophilicity of the compounds since derivatives **9a** and **9j** exhibiting the highest binding affinity had higher calculated partition coefficients (*C*logP) compared to the less active analogues **9b**, **12a** and **14a** with lower *C*logP values (**Table 3**). Overall, these results suggested that hemozoin inhibition is likely one of the mechanisms by which the investigated compounds exert antiplasmodial activity. It is also noteworthy that, with the exception of compound **12a**, all the compounds showed superior hemozoin inhibition compared to the standard drug chloroquine.

DNA binding studies

A majority of Mannich base derivatives such as the α-amino-*o*-cresols explored in the current study have high affinity for DNA.[40-41] This was previously demonstrated with structurally related ferrocenyl 1,3-benzoxazines possessing antiproliferative effects through DNA interaction.[23] Based on our previous findings with structurally similar benzoxazines, it seemed justifiable to interrogate the current Mannich bases, i.e., ferrocenyl α-amino-*o*-cresol analogues, for DNA binding. Using UV-Vis DNA titration experiments, a fixed concentration of calf thymus DNA was incubated with a concentration range of the test compounds (**9a**, **9b**, **9j**, **12a** and **14a**) and the absorbance was monitored at the wavelength of DNA (260 nm).[29, 42] A dose-dependent linear hyperchromic shift accompanied by a slight blue-shift (~ 2 nm) in the spectral maximum of the test samples indicated positive interaction of the compound with DNA via external forces.[43] Only the α-amino-*o*-cresols **9a**, **9b** and **9j** containing the phenolic OH group and rotatable C–NH bond exhibited these effects, while the non-phenolic amine **12a** and

rotationally constrained salicylamide **14a** produced no discernible pattern in the spectral shift of their samples (**Figure 2A-C**).

The data obtained from these results were fitted into the reciprocal guest-host equation (1) relating compound concentration to absorbance to allow quantification of the binding affinity in terms of the binding constant (K_b):

$$\frac{1}{A_c - A_0} = \frac{1}{K_b(A_\infty - A_o)} \times \frac{1}{[C]} + \frac{1}{A_\infty - A_0} \qquad (1)$$

where A_c is absorbance of the DNA sample treated with the compound, A_0 is the absorbance of the untreated DNA sample, $[C]$ is the concentration of the compound, K_b is the binding constant and A_∞ is the hypothetical final absorbance of the DNA-compound complex.[29] The reciprocal plots for compounds **9a**, **9b** and **9j** are illustrated in **Figures 2D-F**.

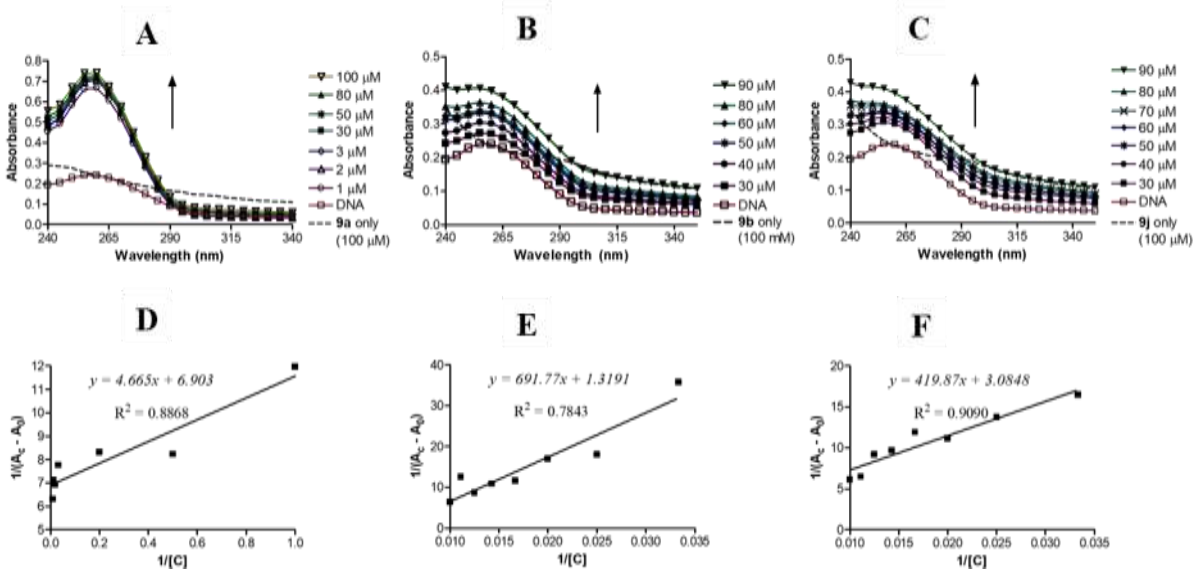

Figure 2 DNA binding results of compounds **9a**, **9b** and **9j**. (**A**) – (**C**) UV-Vis DNA titration spectra of α-amino-*o*-cresols **9a** (**A**), **9b** (**B**) and **9j** (**C**) that produced a dose-dependent hyperchromic effect at 260 nm accompanied by a slight blue shift. (**D**) – (**F**) Guest-host reciprocal plots relating absorbance to compound concentration for α-amino-*o*-cresols **9a** (**D**), **9b** (**E**) and **9j** (**F**).

The binding constant of each compound was determined as the ratio of the slope to *y*-intercept of the equation generated by linear regression.[29] The binding constant for the 4-Me derivative **9b** was 1.91×10^3 M^{-1}, and 1.48×10^6 and 7.35×10^3 M^{-1} for the brominated analogues, **9a** and **9j**, respectively. These findings appeared to be in agreement with the *in vitro* evaluation data of the compounds as compound **9a** with a superior binding constant exhibited both the highest antiplasmodial and antiproliferative potencies in the entire series (**Tables 1** and **2**). The discrepancies in the binding constants of **9b** and **9j** in relation to their *in vitro* antiplasmodial (3D7) and antiproliferative activity may be influenced by possible differences in their ability to penetrate the cells of the targeted diseases as a result of lipophobicity factors, among others. This is supported by the dissimilar *C*logP values of these compounds as presented in **Table 3**, i.e. **9b** *C*logP = 4.24 vs. **9j** *C*logP = 4.97. Notwithstanding, these results demonstrate that one of the possible modalities of the investigated compounds likely involves DNA interaction.

The mode by which an external ligand interacts with a DNA structure is determined by a number of factors such as its size, bonding within the molecule and its orientation in 3D space, i.e., topology, and conformation of the DNA structure. For instance, complex bulky molecules, like natural products azinomycins and pluramycins, tend to bind to the DNA major groove, whereas simple, flat (2D) ligands prefer minor groove binding.[44-45] The UV-Vis DNA titration experiments of the ferrocenyl α-amino-*o*-cresols above merely established that the compounds interact with DNA, possibly via external associations (**Figure 2**). Next in our investigations, we endeavoured to elucidate the mode of interaction by which the compounds bind to DNA using the strongest DNA binder from the UV-Vis titration experiment, i.e., compound **9a**, as a tool compound. Employing previously described Hoechst (DNA minor groove binder) and methylene blue (DNA intercalator) competitive DNA binding assays, interrogation of the binding mode of compound **9a** was undertaken.[23, 46-47] Hoechst 33342, a confirmed DNA minor groove binder, produces an intense fluorescence emission at 460 – 485 nm when bound

to DNA.[48-49] In the presence of a competing DNA minor groove binder, the DNA-bound Hoechst 33342 dye molecules will be competitively displaced from the DNA structure, leading to fluorescence attenuation.[49] On the other hand, methylene blue, which is a strong DNA intercalator, emits strong fluorescence at 660 – 670 nm that gets diminished when the dye is bound to DNA.[50] Compounds that disrupt the DNA-methylene blue intercalation interactions, such as other intercalators, e.g., acridine, or cross-linkers, e.g., cisplatin, lead to an increase in the methylene blue fluorescence emission as more molecules of the dye are liberated from DNA.[23, 51] In our case, the fluorescence emission of the DNA-Hoechst 33342 complex (DNA-Hoechst) was reduced by ~50% upon addition of compound **9a** (100 μM), indicating minor groove binding (**Figure 3A**). On the contrary, addition of 50 and 100 μM of the test compound to the DNA-methylene blue adduct (DNA-MB) did not cause an increase in fluorescence, thus, dismissing **9a** as a DNA intercalator (**Figure 3B**). The methylene blue DNA competitive binding assay was confirmed by adding a DNA cross-linker cisplatin as a positive control to the complex, which intensified the fluorescence of the sample indicating more dye molecules were being displaced from DNA (**Figure 3C**).

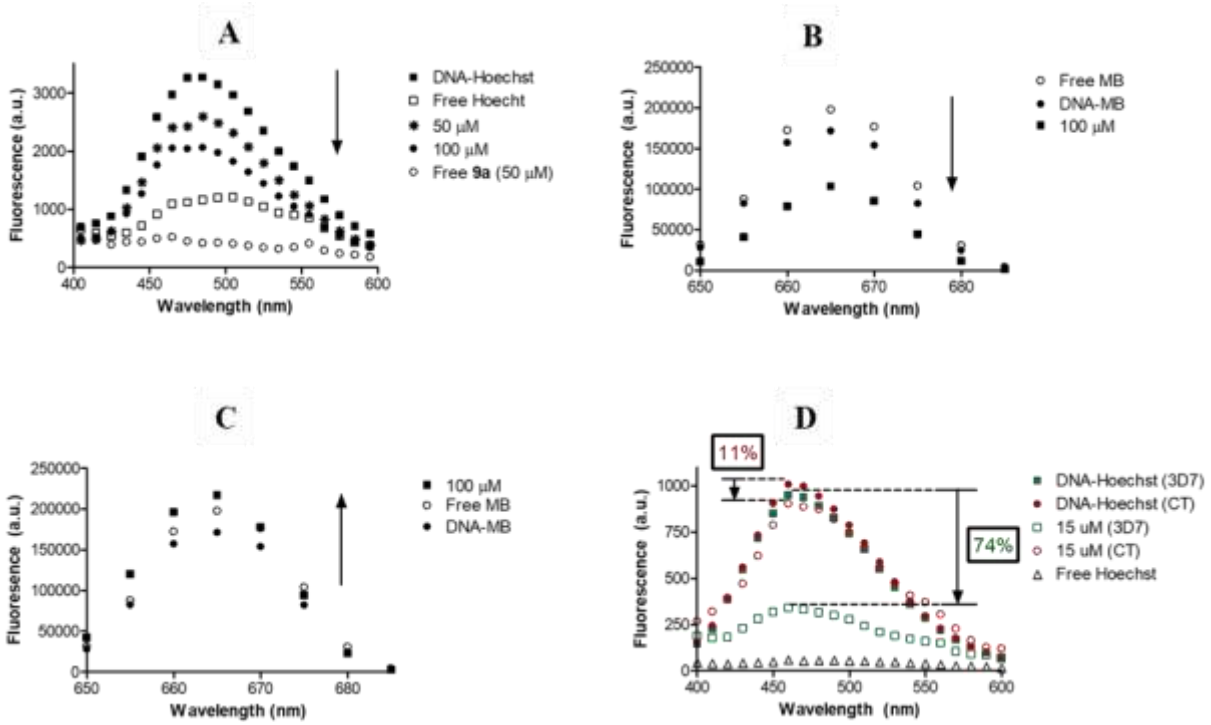

Figure 3 Results of the Hoechst 33342 and methylene blue competitive DNA binding assay for minor groove binding and intercalation. (**A**) Competitive Hoechst 33342 DNA binding results of compound **9a** on calf thymus DNA. (**B**) Competitive methylene blue DNA binding results of compound **9a**. (**C**) Competitive methylene blue DNA binding results of cisplatin. (**D**) Results of the Hoechst assay for selective binding of compound **9a** between mammalian (CT) and malarial (3D7) DNA.

The compounds were generally more selective for the *P. falciparum* strains (3D7 and Dd2) over the mammalian HCC70 triple-negative breast cancer cell line. This preferential efficacy for the malaria parasite seemed justified due to the demonstrated hemozoin inhibitory activity of the compounds which provides complementary modality in addition do DNA interaction, thereby enhancing the antiplasmodial activity of the compounds. However, the genomic differences between mammalian and plasmodial DNA resulting in differences in the composition of the two DNA types, particularly the unusually high AT content of plasmodial DNA, could affect the binding sites for external compounds and provide further explanation

for the marked selectivity of the compounds for the *P. falciparum* parasites over the mammalian HCC70 cancer cells.[52-53] The Hoechst DNA binding assay already validated the compounds as DNA minor groove binders. Using the same assay, we qualitatively assessed the selective binding ability of compound **9a** between the mammalian calf thymus DNA and DNA isolated from 3D7 *P. falciparum* strain. In the assay a 2.5 ng/μL DNA concentration of either mammalian calf thymus DNA (CT) or 3D7 *P. falciparum* DNA (3D7) and Hoechst 33342 (1.0 μg/mL) were incubated with a fixed concentration of **9a** (15 μM) after which fluorescence was monitored as previously described. The results of the assay are illustrated in **Figure 3D**. The test compound induced a significant percentage fluorescence quenching of 74% on the 3D7 DNA-Hoechst complex *vis-à-vis* the calf thymus DNA, which showed 11% fluorescence quenching, decisively demonstrating the preferred binding selectivity of the compounds for the plasmodial DNA over the mammalian DNA. Thus, the enhanced plasmocidal efficacy of the investigated compounds compared to anticancer activity is further explained by their preferential binding to plasmodial DNA over mammalian DNA in addition to hemozoin inhibition.

Furthermore, the electrochemical character of the ferrocene unit is associated with the production of reactive oxygen species (ROS) *in vitro* and *in vivo*,[54] which is essential for biological activity including the induction of DNA damage as documented in previous studies in literature.[55-58] Thus, for future work it would be worthwhile to investigate the electrochemical behaviour of the investigated ferrocenyl compounds in order to provide insight into their ability to produce ROS as a possible complementary mechanistic pathway for their antiplasmodial and antiproliferative activity, in addition to hemozoin binding and DNA interaction.

Computational molecular docking simulations

Computational molecular docking simulations were performed with AutoDock Vina using a computer-generated hemozoin crystal model and a B-DNA structure from protein data bank (PDB code: 1DSI) as biomolecular receptors and *(S)*-planar enantiomers of **9a**, **9j**, **12a** and **14a** as ligands to corroborate the β-hematin and DNA binding experimental data. The model of the hemozoin crystal was constructed as a super cell (3×3×3 unit cell) in BIOVIA Materials Studio 2017 (Dassault Systèmes BIOVIA Materials Studio 2017 v17.1.0.48, San Diego: Dassault Systèmes, 2017) using a resolved X-ray crystal unit of hemozoin (CCDC code: XETXUP01) as a template and optimized according to the parameters reported by Egan and co-workers.[59-60] On the other hand, the DNA receptor (PDB code: 1SDI) was prepared in BIOVIA Discovery Studio Client 2019 (Dassault Systèmes BIOVIA Discovery Studio Client 2019 v19.0.18287, San Diego: Dassault Systèmes, 2019). The binding simulations were run using the AutoDock Vina software package and the results analysed in BIOVIA Discovery Studio Client 2019.[31]

The binding interactions of the compounds with the hemozoin receptor were primarily by non-covalent bonding associations such as van der Waals forces and π-π interactions. In all instances, the compounds bound to the corrugated (001) face and the (010) side face of the hemozoin crystal.[37] The benzene ring of the predicted most stable conformers of the ligands bound to the grooves created between the repeating, stacking hemozoin units on the fast-growing (001) face of the crystal, forming multiple π-π contacts with the protruding, parallel pyrrole rings of the porphyrin subunits (aromatic π-π interactions, 4.30 – 4.75 Å), while the steric bulk and 3D geometry of the ferrocene unit projected this moiety towards the dents between adjacent hemozoin units **(Figure 4A-B**). Aromatic π-π associations were also observed for the latter binding interactions between the ferrocenyl cyclopentadiene rings and the porphyrinoid pyrrole units of the crystal for *(S)*-**9a** (aromatic π-π interactions, 3.834 and 4.472 Å), adding further stabilisation to the complex (**Figure 4A**). Interestingly, the presence

of the 4-Br substituent was favourable for the binding of brominated analogues *(S)*-**9a** and **9j** as shown by the formation of halogen-assisted non-covalent interactions with the porphyrinoid methyl (CH_3) and electron rich methylene ($HC=CH_2$) units of the hemozoin crystal (3.898 – 3.917 Å) (**Figure 4A-B**). The docked structures of the non-brominated analogues **12a** and **14a** lacked these stabilizing interactions in their simulated poses, and their biological activity was inferior to that of **9a** and **9j** containing the 4-Br substituent (**Figure S4A-B**). The beneficial binding effects of the 4-Br substituent in the docking simulations are in agreement with the SAR trends noted for the antiplasmodial and antiproliferative biological data of the investigated compounds.

For the simulated poses that interacted with the (010) side face of the hemozoin crystal, aminocresol *(S)*-**9a** formed a pi-anion interaction (4.609 Å) between the benzene unit and the porphyrin nitrogen atom from hemozoin and a non-classical hydrogen bond ($C=O\cdots CH_3–NCH_3$, 3.678 Å) via the ferrocenyl CH_2NMe_2 moiety with the receptor, underscoring the significance of this motif (**Figure S4C-D**). A classical hydrogen bond was formed between the phenolic oxygen of *(S)*-**9j** and the hemozoin propionic OH group ($HO\cdots HO–CO$, 3.138 Å), adding further stabilization to the adduct. These additional interactions were absent in the non-phenolic benzylamine *(S)*-**12a** and the rotationally limited salicylamide *(S)*-**14a** (**Figure S4E-F**). These observations indicate the pharmacological role of these structural features, i.e., phenolic OH and rotatable C–NH bond, on the biological activity of investigated compounds as previously stated. There was no direct correlation between the observed antimalarial activity of the compounds and the predicted binding energies. However, though comparable, the predicted binding energies of most active forms of the compounds to the hemozoin crystal were below –5 kcal/mol for all the compounds, indicative of stable interactions (**Table 4**).[61] These data seemed to corroborate the findings of the β-hematin binding assay.

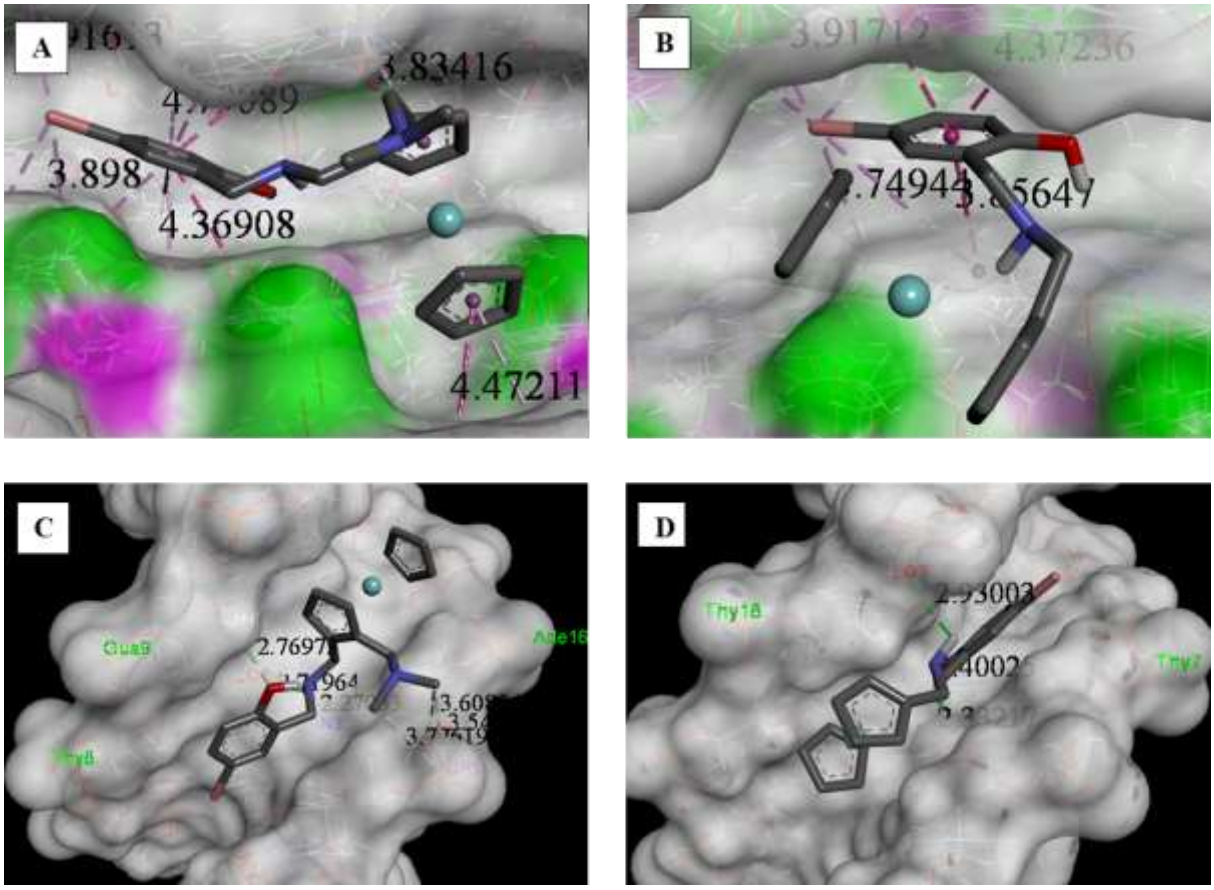

Figure 4 Molecular docking simulation results of aminocresols **9a** and **9j**. Predicated active poses of compound **9a** (**A**) and **9j** (**B**) bound to the corrugated (001) face of the hemozoin crystal. Structures of simulated active conformers of compound **9a** (**C**) and **9j** (**D**) interacting with the DNA minor groove. The labels in black indicate the distance of the binding interactions in angstroms (Å) between the compounds and receptors, and the green annotations represent the DNA bases interacting with the compounds.

For the DNA binding simulations, all the predicted conformations of compounds **9a**, **9j**, **12a** and **14a** exclusively bound to the minor groove of the B-DNA receptor structure, as experimentally determined by the competitive Hoechst 33342 DNA binding assay (**Video 1**). The DNA-compound complexes were mainly stabilized by both classical and non-classical hydrogen bonding between the predicted active conformers of the compounds and the DNA receptor. Classical hydrogen bonding (2.20 – 3.20 Å) with the DNA bases was exhibited by all

the simulated poses of the compounds via either the phenolic OH or aliphatic NH group, whilst non-classical interactions (3.5 – 4.0 Å) were between the phosphate units of the DNA backbone and the Me groups of the ferrocenyl CH_2NMe_2 motif as exemplified by the simulated DNA-bound structures of aminocresols **9a** and **9j** (**Figure 4C-D**). Similar to the hemozoin binding simulation results, the bulky ferrocene unit formed a best fit for the DNA minor groove owing to its 3D shape with the flat benzene ring aligned along the same axis, and the predicted binding energies were all symbolic of stable ligand-receptor interactions (< –5.0 kcal/mol). The simulated binding energies of the compounds seemed to correlate with their observed *in vitro* biological activity. For instance, compound **12a** lacking the hydrogen-bond donating phenolic OH group exhibited inferior binding energy and biological activity compared to the aminocresols **9a** and **9j** endowed with this group (**Table 4**). Additionally, the more favourable binding energy of **9a** (–8.6 kcal/mol) relative to **9j** (–7.3 kcal/mol) was in agreement with both the toxicity of the compounds and their DNA binding constants from UV/Vis titration experiments. These observations appeared to support DNA interaction as a possible mode of action of the investigated compounds.

Table 4 Predicted binding energies of compounds **9a**, **9j**, **12a** and **14a** from the hemozoin and DNA binding simulations.

Compound	Binding energy (kcal/mol)		IC_{50} (μM)	
	Hemozoin	DNA	3D7	HCC70
9a	–7.9	–8.1	1.6 ± 0.04	6.67
9j	–8.4	–7.3	2.3 ± 0.28	na
12a	–7.5	–6.7	2.99 ± 0.30	na
14a	–8.4	–7.2	9.64 ± 1.17	na

In summary, the experimental mechanistic studies were validated using computer-aided molecular docking simulations. The simulated binding interactions between the compounds and the investigated targets, i.e., hemozoin and DNA, provide insight into the role played by the structural features of the compounds, thus confirming the elucidated SAR trends. These findings, together with the experimental mechanistic studies, strongly suggest that the possible mode of action of the α-amino-*o*-cresols pursued in this paper likely involves a combination of hemozoin inhibition and DNA interaction. Additionally, the hemozoin inhibition results and the preferential binding of these compounds to the plasmodial DNA over mammalian DNA are encouraging for further exploration of the presented ferrocenyl chemotypes as dual modal antiplasmodial agents.

CONCLUSION

Herein, we presented the antiplasmodial and anticancer activity of new, structurally simple organometallic compounds assembled by incorporation of the ferrocene unit into the antimalarial α-amino-*o*-cresol scaffold. The compounds showed higher selectivity for the malarial 3D7 and Dd2 strains of the *P. falciparum* parasite, with no indication of cross-resistance, than the human HCC70 breast cancer cells. Comprehensive SAR elucidation of the ferrocenyl α-amino-*o*-cresol structural architecture accomplished by synthesizing rotatable benzylamine and rotationally constrained salicylamide variants revealed that the phenolic OH group and the rotatable C–NH bond are vital for biological activity, possibly due to formation of an intramolecular hydrogen bond. The spectrophotometric DNA titration experiments and β-hematin binding assay, which were supported by *in silico* docking simulations, strongly suggest DNA interaction involving minor groove binding and hemozoin inhibition as plausible mechanistic modalities via which the compounds exert biological activity, thus presenting them as potential antimalarial agents with a dual mode of action. Preferential binding affinity of tool compound **9a** for the plasmodial DNA over the mammalian DNA, together with hemozoin

inhibitory affinity, substantiate the higher selectivity of the compounds for the *P. falciparum* strains. The findings of the current study demonstrate the concept of introducing organometallic complexes into bioactive organic scaffolds as a viable approach to devise novel therapeutic agents with potential to evade or delay the development of clinical resistance by targeting multiple mechanistic pathways. These results support further investigation and development of the studied ferrocenyl aminocresols as antimalarial and anticancer agents.

EXPERIMENTAL

Materials and instrumentation

All the chemicals used in the study were sourced from Merck (South Africa) and used without further purification. The calf thymus DNA was purchased from Thermo Fischer Scientific (South Africa). The 3D7 *P. falciparum* DNA was isolated from cultured 3D7 trophozoites according to the manufacturer's instructions using the Quick-DNA Miniprep Kit (#D3024/D3025) (Zymo Research, Irvine, CA, USA). The progress of each reaction was monitored by thin-layer chromatography on Merck F_{254} silica gel plates and product visualized under ultraviolet light (UV 254 and 366 nm). The melting points of the compounds were determined using the Stuart SMP30 melting point apparatus and were uncorrected. The NMR spectra of the compounds were recorded on Bruker Biospin 400 and 600 MHz NMR spectrometers and the residual signals of chloroform-*d* (7.26 ppm for ^{1}HNMR and 77.16 ppm for ^{13}CNMR) and DMSO-d_6 (2.50 ppm for ^{1}HNMR and 39.52 ppm for ^{13}CNMR) were used as internal references. Assignment of proton signals was achieved by multiplet analysis as well as 2D NMR techniques: COSY and HSQC NMR (**Supporting Information**). The HPLC purity of the compounds was determined on an Agilent 1100 Series HPLC instrument comprised of a reverse-phase Luna® LC column (5 μM C18, 100 Å, 250 × 4.6 mm i.d.), G1315B diode-array detector (DAD), G1311A quaternary pump, G1322A degasser and a G1328B manual injector, and the compounds were run by isocratic elution in 5% NH_4Cl (w/v) buffer (pH 8.0) in acetonitrile for a total running time of 8 minutes. The high-resolution mass spectrometry (HRMS) data were acquired on Waters Synapt G2 Mass Spectrometer (Central Analytical Facility, University of Stellenbosch) using the electrospray ionization (ESI) method set to positive ionization mode. The UV-Vis and fluorescent spectra for DNA binding assays were recorded on a SpectraMax M3 microplate reader (Molecular Devices, San Jose, CA, USA).

General procedure for synthesis of ferrocenyl α-amino-*o*-cresols (9a-m) and benzylamines (12a-b)[26]

To a solution of ferrocenyl amine **7a-b** (1.0. eq.) in EtOH (5 mL) was added an appropriate salicyaldehyde **10a-i** or aldehyde **11a-c** (1.0 eq.) and the resulting suspension was refluxed for 4 hours. Upon completion, the reaction mixture was allowed to cool to room temperature followed by addition of sodium borohydride (2.0 eq.). The reaction mixture was stirred at room temperature for 15 minutes and then refluxed for another 15 minutes. Following cooling to room temperature, 2N HCl solution (2 × 25 mL) was added to extract the product into the aqueous phase and washed with EtOAc (2 × 15 mL). The aqueous layer was basified with 1N NaOH solution (pH 8) and the product extracted with DCM (2 × 25 mL). The collected organic layers were combined, dried (Na_2SO_4) and the solvent was removed under reduced pressure to afford the title compound in high purity. In some cases, the product was purified by column chromatography on basic alumina using gradient elution (DCM → 1:9 MeOH/DCM) to furnish the pure compound.

***N*-2-((*N*,*N*-Dimethylamino)methyl)ferrocenemethyl 4-bromo-α-amino-*o*-cresol (9a)**

Brown viscous oil. Yield: 138.0 mg (41%). ^{1}H NMR (600 MHz, $CDCl_3$) δ 7.24 (d, *J* = 7.6 Hz, 1H, H_5), 7.05 (br s, 1H, H_3), 6.72 (d, *J* = 8.5 Hz, 1H, H_6), 4.12 (s, 2H, FcH), 4.07 – 4.06 (m, 1H, FcH), 4.03 (s, 5H, FcH), 3.84 – 3.79 (m, 3H, $H_{2'a}$, $H_{2''}$), 3.75 (d, *J* = 12.6 Hz, 1H, $H_{1'a}$), 3.31 (d, *J* = 13.5 Hz, 1H, $H_{2'b}$), 2.77 (d, *J* = 12.6 Hz, 1H, $H_{1'b}$), 2.13 (s, 6H, NMe_2); ^{13}C NMR (150 MHz, $CDCl_3$) δ 158.3, 131.3, 131.1, 124.5, 118.3, 110.4, 84.1, 83.9, 71.5, 70.8, 69.2 (5C), 66.1, 58.4, 50.2, 45.9, 44.9 (2C); HRMS (ESI^+) *m/z* calcd for $C_{21}H_{25}BrFeN_2O$: 456.0500, Found 457.0573 $[M+H]^+$; HPLC purity > 82 % (t_R = 3.06 min).

***N*-2-((*N*,*N*-Dimethylamino)methyl)ferrocenemethyl 4-methyl-α-amino-*o*-cresol (9b)**

Brown semi-solid. Yield: 86.5 mg (63%). ^{1}H NMR (600 MHz, $CDCl_3$) δ 6.97 (dd, *J* = 8.1, 1.6 Hz, 1H, H_5), 6.76 (br s, 1H, H_3), 6.74 (d, *J* = 8.1 Hz, 1H, H_6), 4.14 – 4.10 (m, 2H, FcH), 4.05 (t, *J* = 2.4 Hz, 1H, FcH), 4.02 (s, 5H, FcH), 3.82 (d, *J* = 6.0 Hz, 2H, $H_{2''}$), 3.78 (d, *J* = 13.5 Hz, 1H, $H_{1'a}$), 3.72 (d, *J* = 12.6 Hz, 1H, $H_{2'a}$), 3.34 (d, *J* = 13.5 Hz, 1H, $H_{2'b}$), 2.76 (d, *J* = 12.6 Hz, 1H, $H_{1'b}$), 2.25 (s, 3H, Me), 2.12 (s, 6H, NMe_2); ^{13}C NMR (150 MHz, $CDCl_3$) δ 152.7, 131.4, 129.1, 128.0, 126.1, 115.0, 85.2, 71.1, 70.3, 69.0 (5C), 66.1, 58.0, 52.6, 47.2, 45.8, 43.9 (2C); 20.3; HRMS (ESI^+) *m/z* calcd for $C_{22}H_{28}FeN_2O$: 392.1551, Found 393.1632 $[M+H]^+$; HPLC purity > 99% (t_R = 3.04 min).

***N*-2-((*N*,*N*-Dimethylamino)methyl)ferrocenemethyl 4-nitro-α-amino-*o*-cresol (9c)**

Yellow semi-solid. Yield: 98.8 mg (55%). ^{1}H NMR (600 MHz, $CDCl_3$) δ 8.10 – 8.05 (m, 1H, H_5), 7.87 (d, *J* = 2.8 Hz, 1H, H_3), 6.71 (d, *J* = 9.0 Hz, 1H, H_6), 4.16 (br s, 1H, FcH), 4.15 (br s, 1H, FcH), 4.11 (s, 1H, FcH), 4.06 – 4.02 (m, 7H, FcH, $H_{2''}$), 3.89 (d, *J* = 13.6 Hz, 1H, $H_{2'a}$), 3.79 (d, *J* = 13.6 Hz, 1H, $H_{2'b}$), 3.39 (d, *J* = 12.7 Hz, 1H, $H_{1'a}$), 2.79 (d, *J* = 12.7 Hz, 1H, $H_{1'b}$), 2.13 (s, 6H, NMe_2); ^{13}C NMR (150 MHz, $CDCl_3$) δ 136.2, 128.3, 126.0, 125.1, 121.9, 116.8, 83.9 (2C), 71.7, 71.0, 69.2, 69.2 (5C), 66.4, 58.2, 44.7, 44.6 (2C); HRMS (ESI^+) *m/z* calcd for $C_{21}H_{25}FeN_3O_3$: 423.1245, Found 423.1986 $[M+H]^+$; HPLC purity > 93% (t_R = 4.83 min).

***N*-2-((*N*,*N*-Dimethylamino)methyl)ferrocenemethyl α-amino-*o*-cresol (9d)**

Brown semi-solid. Yield: 175.0 mg (95%). ^{1}H NMR (600 MHz, $CDCl_3$) δ 7.17 (t, *J* = 7.7 Hz, 1H, H_5), 6.94 (d, *J* = 7.2 Hz, 1H, H_6), 6.84 (d, *J* = 8.0 Hz, 1H, H_3), 6.77 (t, *J* = 7.4 Hz, 1H, H_4), 4.11 (d, *J* = 2.5 Hz, 2H, $H_{2''}$), 4.05 (t, *J* = 2.5 Hz, 1H, FcH), 4.02 (s, 5H, FcH), 3.86 (d, *J* = 7.9 Hz, 2H, FcH), 3.79 (d, *J* = 13.5 Hz, 1H, $H_{1'a}$), 3.73 (d, *J* = 12.6 Hz, 1H, $H_{2'a}$), 3.34 (d, *J* = 13.5 Hz, 1H, $H_{1'b}$), 2.77 (d, *J* = 12.6 Hz, 1H, $H_{2'b}$), 2.12 (s, 6H, NMe_2); ^{13}C NMR (150 MHz, $CDCl_3$) δ 159.1, 128.5 (2C), 122.6, 118.8, 116.4, 84.6, 84.1, 71.3, 70.7, 69.1 (5C), 66.0, 58.4, 50.8,

45.9, 45.0 (2C); HRMS (ESI^+) *m/z* calcd for $C_{21}H_{26}FeN_2O$: 378.1395, Found 379.1467 $[M+H]^+$; HPLC purity > 99% (t_R = 2.97 min).

***N*-2-((*N*,*N*-Dimethylamino)methyl)ferrocenemethyl 6-methoxy-α-amino-*o*-cresol (9e)**

Light brown viscous oil. Yield: 228.8 mg (76%). ^1H NMR (600 MHz, $CDCl_3$) δ 6.82 (d, *J* = 7.9 Hz, 1H, H_5), 6.75 (t, *J* = 7.8 Hz, 1H, H_4), 6.67 (d, *J* = 7.5 Hz, 1H, H_3), 4.17 (br s, 1H, FcH), 4.13 (br s, 1H, FcH), 4.06 (t, *J* = 2.4 Hz, 1H, FcH), 4.03 (s, 5H, FcH), 3.93 (d, *J* = 6.0 Hz, 1H, $H_{2''a}$), 3.91 (d, *J* = 6.0 Hz, 1H, $H_{2''b}$), 3.88 (s, 3H, OMe), 3.85 (d, *J* = 14.0 Hz, 1H, $H_{2'a}$), 3.77 (d, *J* = 12.7 Hz, 1H, $H_{1'a}$), 3.43 (d, *J* = 14.0 Hz, 1H, $H_{2'b}$), 2.81 (d, *J* = 12.7 Hz, 1H, $H_{1'b}$), 2.12 (s, 6H, NMe_2); ^{13}C NMR (150 MHz, $CDCl_3$) δ 148.0, 147.8, 122.1, 120.9, 118.5, 110.8, 83.8, 83.6, 71.4, 71.0, 69.1 (5C), 66.1, 58.2, 56.0, 49.6, 45.7, 44.8 (2C); HRMS (ESI^+) *m/z* calcd for $C_{22}H_{28}FeN_2O_2$: 408.1500, Found 409.1581 $[M+H]^+$; HPLC purity > 82 % (t_R = 3.23 min).

***N*-2-((*N*,*N*-Dimethylamino)methyl)ferrocenemethyl 6-nitro-α-amino-*o*-cresol (9f)**

Light yellow sticky solid. Yield: 48.2 mg (38%). ^1H NMR (600 MHz, $CDCl_3$) δ 7.90 (d, *J* = 8.2 Hz, 1H, H_5), 7.06 (d, *J* = 6.6 Hz, 1H, H_3), 6.32 (t, *J* = 7.6 Hz, 1H, H_4), 4.48 (d, *J* = 13.1 Hz, 1H, $H_{2'a}$), 4.27 (s, 1H, FcH), 4.19 (d, *J* = 9.2 Hz, 1H, FcH), 4.16 (s, 1H, FcH), 4.12 (s, 5H, FcH), 4.10 – 4.06 (m, 1H, $H_{2'b}$), 3.85 – 3.75 (m, 2H, $H_{2''}$), 3.65 (d, *J* = 12.9 Hz, 1H, $H_{1'a}$), 3.37 (d, *J* = 6.7 Hz, 1H, exch D_2O, NH), 2.88 (d, *J* = 12.8 Hz, 1H, $H_{1'b}$), 2.17 (s, 6H, NMe_2); ^{13}C NMR (150 MHz, $CDCl_3$) δ 135.3, 127.3, 126.6, 125.8, 122.9, 111.6, 83.7, 77.4, 71.9, 71.8, 69.7 (5C), 67.1, 57.7, 47.5, 45.4, 44.3 (2C); HRMS (ESI^+) *m/z* calcd for $C_{21}H_{25}FeN_3O_3$: 423.1245, Found 424.1317 $[M+H]^+$; HPLC purity > 94% (t_R = 4.43 min).

***N*-2-((*N*,*N*-Dimethylamino)methyl)ferrocenemethyl 4,6-dibromo-α-amino-*o*-cresol (9g)**

Red sticky solid. Yield: 170.1 mg (83%). ^1H NMR (600 MHz, $CDCl_3$) δ 7.50 (s, 1H, H_5), 6.96 (s, 1H, H_5), 3 4.16 (s, 2H, FcH) 4.10 (s, 1H, FcH), 4.05 (s, 5H, FcH), 3.98 – 3.91 (m, 2H, $H_{2''}$), 3.82 – 3.77 (m, 2H, $H_{2'a}$, $H_{1'a}$), 3.37 (d, *J* = 13.0 Hz, 1H, $H_{2'b}$), 2.85 (d, *J* = 12.3 Hz, 1H, $H_{1'b}$),

2.18 (s, 6H, NMe_2); ^{13}C NMR (150 MHz, $CDCl_3$) δ 156.3, 133.9, 130.3, 124.3, 112.0, 109.0, 83.0, 82.7, 71.7, 71.2, 69.3 (5C), 66.7, 58.1, 49.7, 45.6, 44.6 (2C); HRMS (ESI^+) *m/z* calcd for $C_{21}H_{24}Br_2FeN_2O$: 533.9605, Found 534.9680 $[M+H]^+$; HPLC purity > 92% (t_R = 7.18 min).

_N_-2-((_N_,_N_-Dimethylamino)methyl)ferrocenemethyl 6-bromo-4-nitro-α-amino-_o_-cresol (9h)

Light orange semi-solid. Yield: 58.6 mg (23%). ^1H NMR (600 MHz, $CDCl_3$) δ 8.46 (d, *J* = 2.8 Hz, 1H, H_5), 7.82 (d, *J* = 2.8 Hz, 1H, H_3), 4.32 (d, *J* = 13.6 Hz, 1H, $H_{2'a}$), 4.27 – 4.26 (m, 1H, FcH), 4.24 (t, *J* = 1.8 Hz, 1H, FcH), 4.21 (t, *J* = 2.5 Hz, 1H, FcH), 4.12 (s, 5H, FcH), 3.89 (d, *J* = 7.5 Hz, 1H, $H_{2''a}$), 3.87 (d, *J* = 7.5 Hz, 1H, $H_{2''b}$), 3.72 (d, *J* = 13.6 Hz, 1H, $H_{2'b}$), 3.64 (d, *J* = 13.1 Hz, 1H, $H_{1'a}$), 2.90 (d, *J* = 13.0 Hz, 1H, $H_{1'b}$), 2.12 (s, 6H, Me_2); ^{13}C NMR (150 MHz, $CDCl_3$) δ 159.6, 142.0, 129.6, 126.2, 123.5, 111.1, 83.7, 77.4, 71.9, 71.8, 69.7 (5C), 67.1, 57.7, 47.5, 45.4, 44.3 (2C); HRMS (ESI^+) *m/z* calcd for $C_{21}H_{24}BrFeN_3O_3$: 501.0350, Found 502.0420 $[M+H]^+$; HPLC purity > 97% (t_R = 3.88 min).

_N_-2-Ferrocenemethyl α-amino-_o_-cresol (9i)

Brown solid. Yield: 293.5 mg (98%). M.p.: 116.5 – 119.0 °C. ^1H NMR (600 MHz, $CDCl_3$) δ 7.19 (br s, 1H, H_5), 7.00 (d, *J* = 7.3 Hz, 1H, H_6), 6.86 (d, *J* = 7.9 Hz, 1H, H_3), 6.79 (br s, 1H, H_4), 4.17 (s, 2H, FcH), 4.15 (s, 2H, FcH), 4.13 (s, 5H, FcH), 4.01 (s, 2H, $H_{2'}$), 3.57 (s, 2H, $H_{1'}$); ^{13}C NMR (150 MHz, $CDCl_3$) δ 158.6, 128.8, 128.5, 122.4, 119.1, 116.5, 85.1, 68.6 (5C), 68.5 (2C), 68.2 (2C), 52.0, 47.5; HRMS (ESI^+) *m/z* calcd for $C_{18}H_{19}FeNO$: 462.1445, Found 463.1656 $[M+H]^+$; HPLC purity > 95% (t_R = 2.37 min).

_N_-2-Ferrocenemethyl 4-bromo-α-amino-_o_-cresol (9j)

Light orange solid. Yield: 180.0 mg (97%). M.p.: 106.5 – 107.2 °C. ^1H NMR (600 MHz, $CDCl_3$) δ 7.24 (br s, 1H, H_5), 7.10 (br s, 1H, H_3), 6.72 (br s, 1H, H_6), 4.15 (s, 4H, FcH), 4.12 (s, 5H, FcH), 3.95 (s, 2H, $H_{2'}$), 3.54 (s, 2H, $H_{1'}$); ^{13}C NMR (150 MHz, $CDCl_3$) δ 157.8, 131.5,

131.2, 124.4, 118.4, 110.8, 84.7, 68.7 (5C), 68.5 (5C), 68.4 (2C), 51.4, 47.5; HRMS (ESI^+) *m/z* calcd for $C_{18}H_{18}BrFeNO$: 398.9921, Found 399.9842 $[M+H]^+$; HPLC purity > 91% (t_R = 5.03 min).

***N*-2-Ferrocenemethyl 6-nitro-*α*-amino-*o*-cresol (9k)**

Light green semi-solid. Yield: 130.0 mg (96%). ^1H NMR (400 MHz, $CDCl_3$) δ 8.10 (d, *J* = 7.7 Hz, 1H, H_5), 7.42 (d, *J* = 7.0 Hz, 1H, H_3), 6.69 (t, *J* = 7.5 Hz, 1H, H_4), 4.59 (s, 2H, $H_{2'}$), 4.24 – 4.15 (m, 9H, FcH), 3.32 (s, 2H, $H_{1'}$); ^{13}C NMR (100 MHz, $CDCl_3$) δ 163.9 (2C), 138.3, 131.6, 120.0, 114.4, 81.8, 69.0 (6C), 68.5, 54.4, 42.4; HRMS (ESI^+) *m/z* calcd for $C_{18}H_{18}FeN_2O_3$: 366.0667, Found 367.0753 $[M+H]^+$; HPLC purity > 87% (t_R = 3.99 min).

***N*-2-Ferrocenemethyl 4,6-dibromo-*α*-amino-*o*-cresol (9l)**

Brown semi-solid. Yield: 314.8 mg (71%). ^1H NMR (600 MHz, $CDCl_3$) δ 7.55 (br s, 1H, H_3), 7.05 (br s, 1H, H_5), 4.18 (s, 2H, FcH), 4.16 (s, 2H, FcH), 4.13 (s, 5H, FcH), 3.96 (s, 2H, $H_{2'}$), 3.56 (s, 2H, $H_{1'}$); ^{13}C NMR (150 MHz, $CDCl_3$) δ 160.7, 135.1, 133.5, 120.3, 1192.3, 110.0, 84.9, 68.8 (5C), 68.2 (2C), 68.0 (2C), 57.9, 48.7; HRMS (ESI^+) *m/z* calcd for $C_{18}H_{17}Br_2FeNO$: 476.9026, Found 477.9099 $[M+H]^+$; HPLC purity > 85% (t_R = 6.99 min).

***N*-2-Ferrocenemethyl 6-bromo-4-nitro-*α*-amino-*o*-cresol (9m)**

Light brown semi-solid. Yield: 241.8 mg (82%). ^1H NMR (600 MHz, DMSO-d_6) δ 8.49 (d, *J* = 2.9 Hz, 1H, H_5), 8.41 (d, *J* = 2.9 Hz, 1H, H_3), 4.63 (s, 2H, $H_{2'}$), 4.33 (t, *J* = 1.8 Hz, 2H, FcH), 4.27 (s, 5H, FcH), 4.24 (t, *J* = 1.8 Hz, 2H, FcH), 4.21 (s, 2H, $H_{1'}$); ^{13}C NMR (150 MHz, DMSO) δ 167.1, 133.1, 132.6, 131.4, 118.3, 111.8, 82.0, 69.4 (2C), 68.7 (5C), 68.5 (2C), 68.0, 50.0; HRMS (ESI^+) *m/z* calcd for $C_{18}H_{17}BrFeN_2O_3$: 443.9772, Found 444.9872 $[M+H]^+$; HPLC purity > 86% (t_R = 2.05 min).

***N*-((*N*,*N*-Dimethylamino)methyl)ferrocenemethyl)methyl benzylamine (12a)**

Brown semi-solid. Yield: 384.0 mg (97%). ^{1}H NMR (600 MHz, $CDCl_3$) δ 7.32 – 7.31 (m, 4H, H_2, H_3), 7.26 – 7.23 (m, 1H, H_4), 4.19 (s, 1H, FcH), 4.10 (s, 1H, FcH), 4.04 (s, 1H, FcH), 4.02 (s, 5H, FcH), 3.84 – 3.78 (m, 2H, $H_{2'a}$, $H_{2''a}$), 3.70 (d, *J* = 13.1 Hz, 1H, $H_{2''b}$), 3.64 (d, *J* = 12.9 Hz, $H_{1'a}$), 3.37 (d, *J* = 13.1 Hz, 1H, $H_{2'b}$), 2.81 (d, *J* = 13.0 Hz, 1H, $H_{1'b}$), 2.09 (s, 6H, NMe_2); ^{13}C NMR (150 MHz, $CDCl_3$) δ 139.5, 128.5 (2C), 128.4 (2C), 127.0 (2C), 85.3, 71.1, 70.3, 69.0 (5C), 66.1, 58.0, 52.6, 46.9, 44.9 (2C); HRMS (ESI^+) *m/z* calcd for $C_{21}H_{26}FeN_2$: 362.1445, Found 363.1527 $[M+H]^+$; HPLC purity > 87% (t_R = 4.59 min).

***N*-((*N*,*N*-Dimethylamino)methyl)ferrocenemethyl)methyl 2-methoxybenzylamine (12b)**

Orange viscous oil. Yield: 45 mg (34%). ^{1}H NMR (400 MHz, $CDCl_3$) δ 6.77 – 6.53 (m, 3H, H_3, H_4, H, H_5), 6.56 – 6.50 (m, 1H, H_6), 4.12 – 4.09 (m, 4H, $H_{2''}$, FcH), 4.04 (br s, 1H, FcH), 4.02 (s, 5H, FcH), 3.82 – 3.78 (m, 2H, $H_{2'}$), 3.75 (s, Hz, 3H, OMe), 3.32 (d, *J* = 13.4 Hz, 1H, $H_{1'a}$), 2.76 (d, *J* = 12.0 Hz, 1H, $H_{1'b}$), 2.11 (s, 6H, NMe_2); ^{13}C NMR (100 MHz, $CDCl_3$) δ 168.8, 157.7, 129.9, 128.4, 120.5, 110.3, 84.0, 83.6, 70.8, 69.4, 69.1 (5C), 69.0, 66.2, 57.9, 55.4, 50.4, 45.0 (2C); HRMS (ESI^+) *m/z* calcd for $C_{22}H_{28}FeN_2O$: 393.1622, Found 393.1623 $[M]^+$; HPLC purity > 95% (t_R = 5.12 min).

***N*-((*N*,*N*-Dimethylamino)methyl)ferrocenemethyl)methyl 2-nitrobenzylamine (12c)**

Brown semi-solid. Yield: 124.2 mg (59%). ^{1}H NMR (600 MHz, $CDCl_3$) δ 7.94 (d, *J* = 8.1 Hz, 1H, H_3), 7.66 (d, *J* = 7.7 Hz, 1H, H_6), 7.58 (t, *J* = 7.5 Hz, 1H, H_4), 7.39 (t, *J* = 7.7 Hz, 1H, H_5), 4.19 (br s, 1H, FcH), 4.12 – 4.10 (m, 1H, FcH), 4.02 (br s, 1H, FcH), 4.05 – 3.99 (m, 7H, FcH, $H_{2''}$), 3.76 (d, *J* = 12.9 Hz, 1H, $H_{2'a}$), 3.61 (d, *J* = 12.6 Hz, 1H, $H_{1'a}$), 3.37 (d, *J* = 12.9 Hz, 1H, $H_{2'b}$), 2.83 (d, *J* = 12.6 Hz, 1H, $H_{1'b}$), 2.09 (s, 6H, NMe_2); ^{13}C NMR (150 MHz, $CDCl_3$) δ 149.1, 136.1, 133.2, 130.8, 127.7, 124.7, 86.2, 83.6, 71.1, 69.9, 69.0 (5C), 66.2, 58.1, 50.0, 47.7, 45.0

(2C); HRMS (ESI$^+$) *m/z* calcd for $C_{21}H_{25}FeN_3O_2$: 407.1296, Found 408.1369 $[M+H]^+$; HPLC purity > 92% (t_R = 7.18 min).

_N_-((_N_,_N_-Dimethylamino)methyl)ferrocenemethyl)methyl 2-aminobenzylamine (12d)[27]

A mixture of 2-nitrobenzylamine **12c** (95.0 mg), zinc dust (126.0 mg) and ammonium chloride (25.0 mg) in methanol (10 mL) was refluxed for 12 hours. Following reflux, the solids were removed through a small pad of silica gel using 1:1 methanol/DCM as an eluent and the filtrate collected and concentrated *in vacuo*. The resulting residue was re-dissolved in EtOAc (25 mL) and then successively washed with saturated $NaHCO_3$ solution and water. The collected organic layer was dried (Na_2SO_3) and the solvent removed under reduced pressure to afford the desired compound as a yellow semi-solid in high purity. Yield: 86.0 mg (98%). ^{1}H NMR (600 MHz, $CDCl_3$) δ 8.69 (d, *J* = 9.0 Hz, 1H, H_3), 7.65 (d, *J* = 8.4 Hz, 1H, H_4), 7.43 – 7.40 (m, 1H, H_5), 7.20 – 7.16 (m, 1H, H_6), 6.55 (d, *J* = 12.1 Hz, 1H, $H_{2''a}$), 5.34 (d, *J* = 12.1 Hz, 1H, $H_{2''b}$), 4.78 (d, *J* = 13.0 Hz, 1H, $H_{2'a}$), 4.25 – 4.24 (m, 6H, FcH), 4.21 (br s, 1H, FcH), 4.17 (t, *J* = 2.5 Hz, 1H, FcH), 4.13 – 4.10 (m, 1H, $H_{2'b}$), 3.08 (d, *J* = 13.0 Hz, 1H, $H_{1'a}$), 2.71 – 2.70 (m, 1H, $H_{1'b}$), 2.29 – 2.20 (m, 6H, NMe_2); ^{13}C NMR (150 MHz, $CDCl_3$) δ 129.6, 127.3, 123.6, 121.5, 120.3, 117.5, 82.6, 79.4, 73.6, 70.0, 69.8 (5C), 69.4, 58.4, 51.8, 49.2, 43.3 (2C); HRMS (ESI$^+$) *m/z* calcd for $C_{21}H_{27}FeN_3$: 377.1554, Found 378.1629 $[M+H]^+$; HPLC purity > 83% (t_R = 4.11 min).

General procedure for the synthesis of ferrocenyl salicylamides (14a-g)[28]

A suspension of an appropriate ferrocenyl amine **7a-b** (1.0 eq.), substituted salicylic acid **13a-f** (1.0 eq.) and DCC (1.2 eq.) pyridine (15 mL) was heated in a monowave microwave reactor at 80 °C for 2 hours. After completion of the reaction, the formed dark brown suspension was kept on ice for 10 minutes, diluted with EtOAc (25 mL) and then filtered through celite to remove the urea precipitate. The filtrate was dried under reduced pressure to give a crude

residue, which was subjected to silica gel column chromatography to afford the pure salicylamide product.

***N*-(*N*,*N*-Dimethylamino)methyl)ferrocenemethyl salicylamide (14a)**

Light brown semi-solid. Yield: 132.0 mg (92%). ^{1}H NMR (400 MHz, $CDCl_3$) δ 7.26 – 7.19 (m, 2H, H_3, H_4), 6.87 (t, *J* = 8.2 Hz, 1H, H_5), 6.69 (br s, 1H, H_6), 4.68 (d, *J* = 13.1 Hz, 1H, $H_{2'a}$), 4.23 – 4.16 (m, 2H, FcH), 4.06 (s, 5H, FcH), 3.99 – 3.94 (m, 2H, FcH, $H_{2'b}$), 3.10 – 3.04 (m, 1H, $H_{1'a}$), 2.83 – 2.79 (m, 1H, $H_{1'b}$), 2.19 (s, 6H, NMe_2); ^{13}C NMR (100 MHz, $CDCl_3$) δ 169.2, 161.8, 133.6, 125.7, 118.3, 118.2, 114.8, 83.9, 71.3, 70.4, 69.6, 69.3 (5C), 66.0, 44.8, 38.3, 29.7 (2C); HRMS (ESI^+) *m/z* calcd for $C_{21}H_{24}FeN_2O_2$: 392.1187, Found 393.1295 $[M+H]^+$; HPLC purity > 80% (t_R = 4.09 min).

***N*-(*N*,*N*-Dimethylamino)methyl)ferrocenemethyl-5-chlorosalicylamide (14b**)

Light yellow semi-solid. Yield: 149.0 mg (95%). ^{1}H NMR (600 MHz, $CDCl_3$) δ 7.26 – 7.25 (m, 2H, H, H_4, H_6), 6.88 (d, *J* = 9.0 Hz, 1H, H_3), 4.71 (d, *J* = 14.4 Hz, 1H, $H_{2'a}$), 4.24 (br s, 1H, FcH), 4.21 (d, *J* = 14.4 Hz, 1H, $H_{2'b}$), 4.14 (br s, 1H, FcH), 4.11 (s, 5H, FcH), 4.05 (t, *J* = 2.4 Hz, 1H, FcH), 3.86 (d, *J* = 12.7 Hz, 1H, $H_{1'a}$), 2.89 (d, *J* = 12.7 Hz, 1H, $H_{1'b}$), 2.29 (s, 6H, NMe_2); ^{13}C NMR (150 MHz, $CDCl_3$) δ 168.0, 160.4, 133.4, 125.8, 123.0, 119.9, 115.8, 83.8, 83.7, 71.6, 70.5, 69.4 (5C), 66.1, 58.4, 44.7 (2C), 38.7; HRMS (ESI^+) *m/z* calcd for $C_{21}H_{23}ClFeN_2O_2$: 426.0797, Found 427.0874 $[M+H]^+$; HPLC purity > 93% (t_R = 4.09 min).

***N*-(*N*,*N*-Dimethylamino)methyl)ferrocenemethyl-5-nitrosalicylamide (14c**)

Yellow semi-solid. Yield: 125.1 mg (78%). ^{1}H NMR (600 MHz, $CDCl_3$) δ 7.56 – 7.53 (m, 2H, H_4, H_6), 6.72 (d, *J* = 9.3 Hz, 1H, H_3), 4.70 (d, *J* = 14.4 Hz, 1H, $H_{2'a}$), 4.23 (br s, 1H, FcH), 4.19 (d, *J* = 14.4 Hz, 1H, $H_{2'b}$), 4.14 (br, 1H, FcH), 4.11 (s, 5H, FcH), 4.05 (t, *J* = 2.4 Hz, 1H, FcH), 3.84 (d, *J* = 12.7 Hz, 1H, $H_{1'a}$), 2.87 (d, *J* = 12.7 Hz, 1H, $H_{1'b}$), 2.33 (s, 6H, NMe_2); ^{13}C NMR (150 MHz, $CDCl_3$) δ 168.0, 137.6, 128.9 (2C), 124.2, 120.1, 114.7, 83.9, 81.9, 71.4, 70.6, 69.5

(5C), 66.8, 58.4, 44.2 (2C), 38.4; HRMS (ESI^+) *m/z* calcd for $C_{21}H_{23}FeN_3O_4$: 437.1038, Found 438.1120 $[M+H]^+$; HPLC purity > 97% (t_R = 2.83 min).

***N*-(*N*,*N*-Dimethylamino)methyl)ferrocenemethyl-4-fluorosalicylamide (14d)**

Light orange semi-solid. Yield: 123.4 mg (82%). ^1H NMR (600 MHz, $CDCl_3$) δ 7.26 – 7.19 (m, 1H, H_3), 6.61 (dd, *J* = 10.5, 2.3 Hz, 1H, H_6), 6.46 (td, *J* = 8.6, 2.3 Hz, 1H, H_5), 4.71 (d, *J* = 14.4 Hz, 1H, $H_{2'a}$), 4.25 (s, 1H, FcH), 4.17 (d, *J* = 14.4 Hz, 1H, $H_{2'b}$), 4.12 (s, 1H, FcH), 4.10 (s, 5H, FcH), 4.04 (s, 1H, FcH), 3.85 (d, *J* = 12.7 Hz, 1H, $H_{1'a}$), 2.88 (d, *J* = 12.7 Hz, 1H, $H_{1'b}$), 2.23 (s, 6H, NMe_2); ^{13}C NMR (150 MHz, $CDCl_3$) δ 168.6, 165.9 (d, *J* = 251.7 Hz), 164.0 (d, *J* = 13.6 Hz), 127.6 (d, *J* = 11.1 Hz), 111.6, 106.1 (d, *J* = 22.6 Hz), 104.9 (d, *J* = 23.3 Hz), 83.9 (2C), 71.4, 70.5, 69.4 (5C), 66.2, 58.2, 44.8 (2C), 38.4; HRMS (ESI^+) *m/z* calcd for $C_{21}H_{23}FeN_2O_2$: 410.1093, Found 410.1010 $[M]^+$; HPLC purity > 99% (t_R = 3.88 min).

***N*-(*N*,*N*-Dimethylamino)methyl)ferrocenemethyl-2-hydroxynicotinamide (14e)**

Light brown semi-solid. Yield: 99.6 mg (69%). ^1H NMR (600 MHz, $CDCl_3$) δ 9.84 (s, 1H, NH), 8.56 (d, *J* = 7.1 Hz, 1H, H_6), 7.30 – 7.25 (m, 1H, H_4), 6.41 (t, *J* = 6.8 Hz, 1H, H_5), 4.49 (dd, *J* = 15.0, 5.7 Hz, 1H, $H_{2'a}$), 4.31 (dd, *J* = 15.0, 3.8 Hz, 1H, $H_{2'b}$), 4.24 (br s, 1H, FcH), 4.23 (br s, 1H, FcH), 4.16 (s, 5H, FcH), 4.10 (t, *J* = 2.1 Hz, 1H, FcH), 3.51 (d, *J* = 13.0 Hz, 1H, $H_{1'a}$), 3.31 (d, *J* = 13.0 Hz, 1H, $H_{1'b}$), 2.20 (s, 6H, NMe_2); ^{13}C NMR (150 MHz, $CDCl_3$) δ 163.8, 163.5, 145.3, 138.1, 121.3, 107.7, 85.3, 82.4, 70.7, 69.3, 68.5 (2C), 67.1, 57.1, 44.8 (2C), 37.7; HRMS (ESI^+) *m/z* calcd for $C_{20}H_{23}FeN_3O_2$: 393.1140, Found 394.1221 $[M+H]^+$; HPLC purity > 98% (t_R = 3.50 min).

***N*-Ferrocenemethylsalicylamide (14f)**

Orange semi-solid. Yield: 218.2 mg (70%). ^1H NMR (400 MHz, $CDCl_3$) δ 12.37 (br s, 1H, OH), 7.40 (t, *J* = 8.4 Hz, 1H, H_4), 7.32 (d, *J* = 8.0 Hz, 1H, H_6), 7.00 (d, *J* = 8.3 Hz, 1H, H, H_3), 6.84 (t, *J* = 7.9 Hz, 1H, H_5), 6.49 (br s, 1H, NH), 4.32 (d, *J* = 5.1 Hz, 2H, $H_{1'}$), 4.26 – 4.25 (m,

2H, FcH), 4.21 (s, 5H, FcH), 4.20 – 4.18 (m, 2H, FcH); ^{13}C NMR (100 MHz, $CDCl_3$) δ 169.3, 161.7, 134.3, 125.2, 118.8 (2C), 114.2, 84.1, 68.7 (2C), 68.5 (7C), 39.1; HRMS (ESI^+) *m/z* calcd for $C_{18}H_{17}FeNO_2$: 335.0609, Found 335.0601 $[M]^+$; HPLC purity > 99% (t_R = 2.14 min).

***N*-Ferrocenemethylthiosalicylamide (14g)**

Brown semi-solid. Yield: 222.1 mg (68%). ^{1}H NMR (600 MHz, $CDCl_3$) δ 8.02 (d, *J* = 7.8 Hz, 1H, H_6), 7.55 (t, *J* = 7.4 Hz, 1H, H_4), 7.46 (d, *J* = 8.0 Hz, 1H, H_3), 7.36 (t, *J* = 7.4 Hz, 1H, H_5), 4.82 (s, 2H, $H_{1'}$), 4.33 (s, 2H, FcH), 4.21 (s, 5H, FcH), 4.19 (s, 2H, FcH); ^{13}C NMR (150 MHz, $CDCl_3$) δ 164.9, 140.4, 131.7, 126.8, 125.5, 124.9, 120.4, 82.1, 69.6 (2C), 69.0 (7C), 43.6; HRMS (ESI^+) *m/z* calcd for $C_{18}H_{17}FeNOS$: 351.0380, Found 351.0269 $[M]^+$; HPLC purity > 99% (t_R = 3.37min).

3D7 *Plasmodium falciparum* antiplasmodial assay

The malaria parasites (3D7 *P. falciparum* strain) were cultured in a medium RPMI1640 containing 25 mM L-glutamine, 25 mM HEPES (Lonza, Switzerland), 0.5% (w/v) albumax II (Thermo Fisher Scientific, Waltham, MA), 20 mM glucose, 0.65 mM hypoxanthine, 60 μg/mL gentamicin and 2 – 4 % (v/v) hematocrit erythrocytes. The cultures were maintained at 37 °C under an atmosphere of 5% CO_2, 5% O_2 and 90% N_2, and then were treated with three-fold serial dilutions of the test compounds and chloroquine (control) in 96-well plates. The plates were incubated under the same conditions for 48 hours after which 20 μL of the culture was removed from each well and transferred to a new plate. The transferred cultures were mixed with 125 μL of a mixture of Malstat and nitroblue tetrazolium/phenazine ethosulfate solution to assess the activity of the plasmodium lactate dehydrogenase (pLDH) enzyme in the cultures by measuring absorbance at 620 nm on the SpectraMax M3 microplate reader (Molecular Devices, San Jose, CA, USA). To quantify the antiplasmodial activity of the compounds, the recorded absorbance of the formed purple product in each well was plotted against the

logarithm of the corresponding compound concentration in GraphPad Prism 5.02 software and the plasmocidal activities were reported as half-maximal inhibitory concentration (IC_{50}) by non-linear regression analysis.[62] The activity was determined in duplicate for each compound.

Dd2 *Plasmodium falciparum* antiplasmodial assay

Cultures of the Dd2 *P. falciparum* strain were prepared and maintained in an Albumax II-containing medium (Thermo Fisher Scientific, South Africa) according to a modified procedure by Trager and Jensen, keeping the hematocrit concentration at 4%.[63] Upon reaching the trophozoite stage, the cultures were seeded in 96-well plates and incubated with varying concentrations of the test compounds (0 – 10 μM) and controls (chloroquine and artemisinin). The plates were incubated for 48 hours under an atmosphere containing 4% CO_2 and 3% O_2 in nitrogen at 37 °C. The pLDH procedure was employed to determine the antiplasmodial activity of the compounds in triplicate as previously reported.[64-65]

HeLa assay for preliminary cytotoxicity testing

Cultures of HeLa cells (Cellonex, South Africa) were grown in Dulbecco's Modified Eagle's medium (Lonza, Switzerland) containing 10% foetal calf serum and antibiotics (penicillin, streptomycin and amphotericin B) in a 5% CO_2 incubator maintained at 37 °C. The cells were seeded in a 96-well pate and incubated for 24 hours. After incubation, the test compounds were added to the seeded cells in the wells to a final concentration of 20 μM and further incubated for 48 hours under the same conditions. The viability of the cells in each well was determined using the resazurin procedure previously reported by reading the resorufin fluorescence in a SpectraMax M3 microplate reader.[36]

HCC70 breast cancer cell line antiproliferative assay

The HCC70 human triple-negative breast cancer cells were cultured in RPMI media supplemented with 10% (v/v) foetal bovine serum (FBS), 1 mM L-glutamine, 100 U/mL

penicillin, 100 µg/mL streptomycin and 12.5 µg/mL amphotericin (PSA) and were maintained at 37 °C in a 9% CO_2 atmosphere. The cells were seeded in 96-well plates with cell density adjusted to 5×10^3 cells/well and allowed to adhere to the plate overnight. A concentration range (0 – 1000 µM) of either the paclitaxel (positive control) or test compounds in DMSO was added to the seeded cell and incubated for 72 hours under the same atmosphere. The antiproliferative activity of the compounds was determined using a previously described resazurin assay.[23] IC_{50} values were calculated by non-linear regression using GraphPad Prism 4.0 software.

UV-Vis DNA titration experiment

A concentration range of 0 – 100 µM of the test compounds (**9a**, **9b**, **9j**, **12a** and **14a**) prepared from a 20 mM stock solution in DMSO using milli-Q water were added to a solution of calf thymus DNA (70 ng/µL) in a 96-well pate and incubated at 37 °C for 15 minutes. Following incubation, the absorbance of the samples in each well was monitored between 230 and 290 nm on a SpectraMax M3 microplate plate reader (Molecular Devices, San Jose, CA, USA). The absorbance of a 100 µM sample of each test compound was also recorded in the same wavelength range. To assess the binding affinity of the compounds for DNA, the concentration-dependent response curves of the samples were plotted as spectra depicting absorbance measured over wavelengths from 230 to 290 nm. The binding affinity of the compounds was determined in terms of the binding constant as the ratio of intercept to slope of the reciprocal guest-host plot correlating maximum absorbance (around 260 nm) to compound concentration.

Competitive DNA binding studies

A solution of Hoechst 33342 (1 µg/mL) or methylene blue (1.5 µg/mL) was added to a solution of calf thymus DNA (70 µg/mL) containing 0 (i.e., DMSO), 50 or 100 µM of test compounds **9a** and **9j** in milli-Q water. The samples were allowed to equilibrate in the dark at room temperature for 15 minutes after which fluorescence spectra were recorded (excitation: 350

nm, emission: 400 – 600 nm for Hoechst 33342 and excitation: 665 nm, emission: 650 – 750 nm for methylene blue). A 100 μM sample of cisplatin prepared similarly to the test sample was employed as a positive control in the competitive methylene blue intercalation study.

Selective DNA binding assay between malarial and mammalian DNA

The selective binding assay was carried out as described for the Hoechst assay above using 15 μM of compound **9a**, 2.5 ng/μL calf-thymus DNA and 2.5 ng/μL DNA isolated from the 3D7 *P. falciparum*. Isolation of the malarial DNA was accomplished with the Quick-DNA Miniprep Kit (#D3024/D3025) (Zymo Research, Irvine, CA, USA) according to the manufacturer's instructions and literature methods using 3D7 *P. falciparum* trophozoites cultured similarly to those employed in the 3D7 antiplasmodial evaluation assay as a DNA source.[66]

β-Hematin binding assay

Hemozoin inhibitory assay was performed according the procedure reported by Egan and co-workers with minor modifications.[38] A 25 μM stock solution of β-hematin was prepared by dissolving 25 mg of hemin (from porcine) in 947 μL of DMSO and sonicating the resulting suspension for 1 minute to ensure complete homogenization. A volume of 178 μM of the hematin solution was added to 20 mL of 1.0 M acetate buffer (pH 4.8) and thoroughly mixed to give a final concentration of 220 μM hematin solution. Varying concentrations (1 – 1000 μM) of the test compounds (**9a**, **9b**, **9j**, **12a** and **14a)** in DMSO were placed in a 96-well plate, keeping the total volume of DMSO below 10 μL in each well. A sample of chloroquine was prepared similarly and used as a positive control in the assay, while DMSO was used as a negative control. The samples were treated with 100 μL of the 220 μM hematin solution in acetate 20 μL and 30 μM NP-40 detergent was added to induce hemozoin formation. This was followed by addition of 70 μL of deionised water to give a final volume of 200 μM in each well. The plate was incubated at 37 °C for 6 hours with gentle shaking. After 6 hours, the

analysis of hemozoin formation was carried out according to the pyridine-ferrichrome method by Ncokazi and Egan by adding to each well a solution of 50% pyridine (v/v), 20% acetone (v/v), 10% distilled water and 20% 200 mM HEPES buffer (pH 7.4).[30] The plate was further incubated for 10 minutes with gentle shaking followed by addition of 50 μL acetone to facilitate hemozoin dispersion. Absorbance was measured at 605 nm for each well and plotted against a logarithm of the corresponding concentration on GraphPad Prism 4.0. Sigmoidal non-linear regression analysis was performed to quantify hemozoin inhibition of each compound in terms IC_{50} values.

Computational docking simulations

The model of the hemozoin crystal was constructed with the supercell builder tool (3×3×3 unit cell) in BIOVIA Materials Studio 2017 (Dassault Systèmes BIOVIA Materials Studio 2017 v17.1.0.48, San Diego: Dassault Systèmes, 2017) using the resolved X-ray crystal structure of hemozoin (CCDC code: XETXUP01) as a template.[60] The model was optimized according to the parameters reported by Egan and colleagues before it was used in the *in silico* docking simulations.[59] The B-DNA structure was obtained from protein data bank (PDB code: 1DSI) and prepared in BIOVIA Discovery Studio Client 2019 (Dassault Systèmes BIOVIA Discovery Studio Client 2019 v19.0.18287, San Diego: Dassault Systèmes, 2019) for docking simulations. Ligand structures of the investigated compounds (**9a**, **9j**, **12a** and **14a**) were prepared as *(S)*-planar enantiomers and minimized in Chem3D Pro 12.0, applying a minimum RMSD gradient of 0.010. The docking simulations were performed using AutoDock Vina software package and the results were analyzed in BIOVIA Discovery Studio Client 2019 and the binding energies were reported in kcal/mol.[31]

ACNOWLEDGEMENTS

The authors gratefully acknowledge the Rhodes University Sandisa Imbewu Grant (SDK, HCH, JDLM and ALE), the National Research Foundation of South Africa (MM, LMKD, TS, DC, JL, JDM, HCH, ALE, SDK) for financial support and Thuthuka National Research Foundation (Grant No. 107270, SDK). The South African Research Chairs Initiative of the Department of Science and Technology and National Research Foundation of South Africa (Grant No. 98566) and National Research Foundation CPRR (Grant No. 105829) is also acknowledged for financial assistance (ALE). The antiplasmodial and HeLa cytotoxicity bioassay component of the project were funded by the South African Medical Research Council (SAMRC). The authors thank Professor Gilles Lemercier (Université de Reims Champagne-Ardenne) for his advice regarding the prediction of the partition coefficients.

Keywords: Ferrocene, Aminocresols, Aminomethylphenols, *Plasmodium falciparum*, Triple-negative breast cancer, Hemozoin inhibition, DNA interaction.

REFERENCES

[1] M. M. Gottesman, *Annu. Rev. Med.* **2002**, *53*, 615-627.

[2] B. C. Baguley, *Mol. Biotechnol.* **2010**, *46*, 308-316.

[3] G. Housman, S. Byler, S. Heerboth, K. Lapinska, M. Longacre, N. Snyder, S. Sarkar, *Cancers* **2014**, *6*, 1769-1792.

[4] M. Nikolaou, A. Pavlopoulou, A. G. Georgakilas, E. Kyrodimos, *Clin. Exp. Metastasis* **2018**, *35*, 309-318.

[5] P. Olliaro, *Pharmacol. Ther.* **2001**, *89*, 207-219.

[6] M. A. Saifi, T. Beg, A. H. Harrath, F. S. H. Altayalan, S. Al Quraishy, *Afr. J. Pharm. Pharmacol.* **2013**, *7*, 148-156.

[7] D. J. Krogstad, I. Y. Gluzman, D. E. Kyle, A. Oduola, S. K. Martin, W. K. Milhous, P. H. Schlesinger, *Science* **1987**, *238*, 1283-1285.

[8] M. Foley, L. Tilley, *Pharmacol. Ther.* **1998**, *79*, 55-87.

[9] E. Proschak, H. Stark, D. Merk, *J. Med. Chem.* **2018**, *62*, 420-444.

[10] M. d. Oliveira Pedrosa, D. da Cruz, R. Marques, J. d. Oliveira Viana, R. O. de Moura, H. M. Ishiki, F. Barbosa, J. Maria, M. F. Diniz, M. T. Scotti, *Curr. Top. Med. Chem.* **2017**, *17*, 1044-1079.

[11] C. Herrera Acevedo, L. Scotti, M. F. Alves, M. de FFM Diniz, M. Tullius Scotti, *Lett. Org. Chem.* **2019**, *16*, 81-92.

[12] M. Patra, G. Gasser, *Nat. Rev. Chem* **2017**, *1*, 0066.

[13] G. Jaouen, A. Vessières, S. Top, *Chem. Soc. Rev.* **2015**, *44*, 8802-8817.

[14] A. Singh, I. Lumb, V. Mehra, V. Kumar, *Dalton Trans.* **2019**, *48*, 2840-2860.

[15] A. Kondratskyi, K. Kondratska, F. V. Abeele, D. Gordienko, C. Dubois, R.-A. Toillon, C. Slomianny, S. Lemière, P. Delcourt, E. Dewailly, R. Skryma, C. Biot, N. Prevarskaya, *Sci. Rep.* **2017**, *7*, 1-15.

[16] C. N. Morrison, K. E. Prosser, R. W. Stokes, A. L. Cordes, N. Metzler-Nolte, S. M. Cohen, *Chem. Sci.* **2020**.

[17] A. W. Hung, A. Ramek, Y. Wang, T. Kaya, J. A. Wilson, P. A. Clemons, D. W. Young, *Proc. Natl. Acad. Sci. U.S.A.* **2011**, *108*, 6799-6804.

[18] J. Burckhalter, F. Tendick, E. M. Jones, W. Holcomb, A. Rawlins, *J. Am. Chem. Soc.* **1946**, *68*, 1894-1901.

[19] L. Schmidt, R. Crosby, *Antimicrob. Agents Chemother.* **1978**, *14*, 672-679.

[20] M. Chinnapattu, K. I. Sathiyanarayanan, P. S. Iyer, *Bioorg. Med. Chem. Lett.* **2015**, *25*, 952-955.

[21] H. D. Attram, S. Wittlin, K. Chibale, *MedChemComm* **2019**, *10*, 450-455.

[22] Medicines for Malaria Venture. Developing antimalarials to save lives. Malaria Box Research, https://www.mmv.org/mmv-open/malaria-box/malaria-box-research, Accessed: 19 November 2019.

[23] M. Mbaba, L. M. Dingle, D. Cash, J.-A. de la Mare, D. Laming, D. Taylor, H. C. Hoppe, A. L. Edkins, S. D. Khanye, *Eur. J. Med. Chem.* **2020**, *187*, 111924.

[24] C. Biot, G. Glorian, L. A. Maciejewski, J. S. Brocard, O. Domarle, G. Blampain, P. Millet, A. J. Georges, H. Abessolo, D. Dive, *J. Med. Chem.* **1997**, *40*, 3715-3718.

[25] T. Stringer, H. Guzgay, J. M. Combrinck, M. Hopper, D. T. Hendricks, P. J. Smith, K. M. Land, T. J. Egan, G. S. Smith, *J. Organomet. Chem.* **2015**, *788*, 1-8.

[26] A. F. Abdel-Magid, K. G. Carson, B. D. Harris, C. A. Maryanoff, R. D. Shah, *J. Org. Chem.* **1996**, *61*, 3849-3862.

[27] B. Saikia, *Synlett* **2011**, *17*, 2597-2598.

[28] F. Mu, D. J. Lee, D. E. Pryor, E. Hamel, M. Cushman, *J. Med. Chem.* **2002**, *45*, 4774-4785.

[29] S. T. Saito, G. Silva, C. Pungartnik, M. Brendel, *J. Photochem. Photobiol. B* **2012**, *111*, 59-63.

[30] K. K. Ncokazi, T. J. Egan, *Anal. Biochem.* **2005**, *338*, 306-319.

[31] O. Trott, A. J. Olson, *J. Comput. Chem.* **2010**, *31*, 455-461.

[32] P. M. O'Neill, S. A. Ward, N. G. Berry, J. P. Jeyadevan, G. A. Biagini, E. Asadollaly, B. K. Park, P. G. Bray, *Curr. Top. Med. Chem.* **2006**, *6*, 479-507.

[33] P. B. Madrid, A. P. Liou, J. L. DeRisi, R. K. Guy, *J. Med. Chem.* **2006**, *49*, 4535-4543.

[34] F. Dubar, T. J. Egan, B. Pradines, D. Kuter, K. K. Ncokazi, D. Forge, J.-F. Paul, C. Pierrot, H. Kalamou, J. Khalife, E. Buisine, C. Rogier, H. Vezin, I. Forfar, C. Slomianny, X. Trivelli, S. Kapishnikov, L. Leiserowitz, D. Dive, C. Biot, *ACS Chem. Biol.* **2011**, *6*, 275-287.

[35] S. Mundra, V. Thakur, A. M. Bello, S. Rathore, M. Asad, L. Wei, J. Yang, S. K. Chakka, R. Mahesh, P. Malhotra, *Bioorg. Med. Chem.* **2017**, *25*, 5662-5677.

[36] R. M. Beteck, L. J. Legoabe, M. Isaacs, S. D. Khanye, D. Laming, H. C. Hoppe, *Medicina* **2019**, *55*, 206.

[37] R. Buller, M. L. Peterson, O. Almarsson, L. Leiserowitz, *Cryst. Growth Des.* **2002**, *2*, 553-562.

[38] W.-J. Lu, K. J. Wicht, L. Wang, K. Imai, Z.-W. Mei, M. Kaiser, I. E. T. El Sayed, T. J. Egan, T. Inokuchi, *Eur. J. Med. Chem.* **2013**, *64*, 498-511.

[39] T. Stringer, D. Taylor, C. de Kock, H. Guzgay, A. Au, S. H. An, B. Sanchez, R. O'Connor, N. Patel, K. M. Land, *Eur. J. Med. Chem.* **2013**, *69*, 90-98.

[40] G. Roman, *Eur. J. Med. Chem.* **2015**, *89*, 743-816.

[41] J. Dimmock, P. Kumar, *Curr. Med. Chem.* **1997**, *4*, 1-22.

[42] N. Shahabadi, S. Hadidi, *Spectrochim. Acta A* **2012**, *96*, 278-283.

[43] M. Sirajuddin, S. Ali, A. Badshah, *J. Photochem. Photobiol. B* **2013**, *124*, 1-19.

[44] P. L. Hamilton, D. P. Arya, *Nat. Prod. Rep.* **2012**, *29*, 134-143.

[45] A. Lauria, A. Montalbano, P. Barraja, G. Dattolo, A. M. Almerico, *Curr. Med. Chem.* **2007**, *14*, 2136-2160.

[46] N. Shahabadi, S. Hadidi, A. A. Taherpour, *Appl. Biochem. Biotechnol.* **2014**, *172*, 2436-2454.

[47] N. Shahabadi, M. Maghsudi, *Mol. BioSyst.* **2014**, *10*, 338-347.

[48] J. Bucevičius, G. Lukinavičius, R. Gerasimaitė, *Chemosensors* **2018**, *6*, 18.

[49] L. C. Sandhu, R. L. Warters, L. A. Dethlefsen, *Cytometry A* **1985**, *6*, 191-194.

[50] P. Vardevanyan, A. Antonyan, M. Parsadanyan, M. Shahinyan, L. Hambardzumyan, *J. Appl. Spectrosc.* **2013**, *80*, 595-599.

[51] S. Nafisi, A. A. Saboury, N. Keramat, J.-F. Neault, H.-A. Tajmir-Riahi, *J. Mol. Struct.* **2007**, *827*, 35-43.

[52] L. Aravind, L. M. Iyer, T. E. Wellems, L. H. Miller, *Cell* **2003**, *115*, 771-785.

[53] J. M. Woynarowski, M. Krugliak, H. Ginsburg, *Mol. Biochem. Parasitol.* **2007**, *154*, 70-81.

[54] M. Patra, G. Gasser, *Nat. Rev. Chem* **2017**, *1*, 1-12.

[55] Y. L. K. Tan, P. Pigeon, S. Top, E. Labbé, O. Buriez, E. A. Hillard, A. Vessières, C. Amatore, W. K. Leong, G. Jaouen, *Dalton Trans.* **2012**, *41*, 7537-7549.

[56] C. Lu, J. M. Heldt, M. Guille-Collignon, F. Lemaître, G. Jaouen, A. Vessières, C. Amatore, *ChemMedChem* **2014**, *9*, 1286-1293.

[57] C. Acevedo-Morantes, E. Meléndez, S. Singh, J. Ramírez-Vick, *J. Cancer Sci. Ther.* **2012**, *4*, 271-275.

[58] M. Maschke, J. Grohmann, C. Nierhaus, M. Lieb, N. Metzler-Nolte, *ChemBioChem* **2015**, *16*, 1333-1342.

[59] F. P. L'abbate, R. Müller, R. Openshaw, J. M. Combrinck, K. A. de Villiers, R. Hunter, T. J. Egan, *Eur. J. Med. Chem.* **2018**, *159*, 243-254.

[60] D. S. Bohle, E. L. Dodd, P. W. Stephens, *Chem. Biodivers.* **2012**, *9*, 1891-1902.

[61] O. Takahashi, Y. Masuda, A. Muroya, T. Furuya, *SAR QSAR Environ. Res.* **2010**, *21*, 547-558.

[62] M. Mbaba, A. N. Mabhula, N. Boel, A. L. Edkins, M. Isaacs, H. C. Hoppe, S. D. Khanye, *J. Inorg. Biochem.* **2017**, *172*, 88-93.

[63] W. Trager, J. B. Jensen, *Science* **1976**, *193*, 673-675.

[64] O. O. Oderinlo, M. Tukulula, M. Isaacs, H. C. Hoppe, D. Taylor, V. J. Smith, S. D. Khanye, *Appl. Organomet. Chem.* **2018**, *32*, e4385.

[65] M. T. Makler, D. J. Hinrichs, *Am. J. Trop. M. Hyg.* **1993**, *48*, 205-210.

[66] H. Wu, M. K. de Gannes, G. Luchetti, J. R. Pilsner, *Biotechniques* **2015**, *58*, 293-300.